Journal of Marine Research, 58, 919–956, 2000

Islands as eddy splitters

by Harper Lightfoot Simmons[1] and Doron Nof[2]

ABSTRACT

Previous theoretical work has shown that, in an unbounded domain, anticyclones are prohibited from splitting on their own due to limitations imposed by the conservation of angular momentum. By explicitly considering the role of angular momentum exchange between eddies and boundaries (neglected by previous theories), splitting criteria for an anticyclonic lens colliding with a long and thin island are established analytically. The inviscid analytical model consists of an isolated patch of fluid in a reduced gravity regime. Nonlinear analytical solutions are constructed by connecting the initial and final states using conserved quantities (integrated angular momentum, vorticity and mass) and the familiar slowly varying approximation.

For the conceptual case of a lens pierced by a thin moving wall, the result is that, in order for a zero potential vorticity lens (with a radius R_1) to split into two equal offspring, the wall length must be at least $1.19R_1$. Even for infinitesimal splitting, which arises from weak collisions (where the wall merely "brushes" the lens), the wall must be $O(R_1)$. This is because the "parent" lens can split into two offspring only when the wall allows sufficient spreading of the lens, which increases its relative angular momentum, and thereby enables the lens to form two distinct "offspring."

Numerical experiments employing Lagrangian floats reveal that the splitting is accomplished by a jet that leaks fluid along the wall, forming a second lens. The fluid initially found along the rim of the parent lens occupies both the core and the rim of the second lens; the fluid found at an intermediate radius in the second lens is derived from fluid situated at an intermediate radius in the parent lens. In general, a very good agreement between the numerics and the analytical theory is found. The numerical simulations demonstrate that the integrated angular momentum is a far stronger constraint than energy conservation. Using the numerics, we extend the moving wall theory to the splitting of finite vorticity lenses and lenses on a β-plane. We find that the basic requirement of mass redistribution by a wall is relevant in all the regimes that we examined, and, therefore, is likely to also be relevant to collisions of eddies with actual islands. This supports our application of the theory to Meddy splitting by seamounts, where we find that the seamounts can provide the necessary torque for the recently observed Meddy splitting and destruction.

1. Introduction

Oceanographers are interested in eddy fission (splitting) because of the associated transfer of energy, momentum, salinity, and temperature to small, dissipative scales. There

1. School of Earth and Ocean Sciences, University of Victoria, Box 3055, Victoria, BC, Canada, V8W 3P6. ***email: harper@ocean.seos.uvic.ca***

2. Department of Oceanography and The Geophysical Fluid Dynamics Institute, Florida State University, Tallahassee, Florida, 32306-4320, U.S.A.

have been no observations of anticyclones breaking up in the open ocean and Nof (1990, 1991) argued that, while cyclones can easily split, anticyclones in the open ocean are prohibited from splitting on their own. One possible cause of eddy destruction is by collisions with topography (see, e.g., Richardson *et al.,* 1989 and Richardson and Tychensky, 1998) and this is the focus of our study.

a. Definition of the problem

It seems obvious that an eddy's collision with very small obstructions cannot result in fission (e.g., a 400 km North Brazil Current Ring and a boat), whereas very large obstacles (e.g., the collision of a Meddy with a seamount of the same scale—see Fig. 1) might be associated with splitting. Therefore, as a first crack at determining what sorts of collisions between eddies and islands may result in lens destruction, we ask the question: how big must an island be before it can break up an intense nonlinear eddy? To address this question, we consider a simplified inviscid reduced gravity model (Fig. 2). The eddy will be represented by an isolated lens of fluid in a reduced gravity regime. Our model represents a patch of dense water resting on the bottom below an infinitely deep upper layer, an intra-thermocline eddy (such as a Meddy), or a surface warm core ring such as are shed by the Gulf Stream, North Brazil Current, and the Agulhas Current. We use Conservation of Integrated Angular Momentum (CIAM), which, as we will show, strongly constrains the breakage of lenses and explicitly accounts for the required external torques. Additional constraints are potential vorticity (PV) and mass conservation. As is the case in familiar adjustment problems, energy is not conserved during the lens splitting; rather, it must be radiated away in the form of long gravity waves. The island geometry is simplified to that of a thin (vertical) wall of finite length. The treatment of more general island geometries is beyond the scope of this investigation; a companion paper considers the passage of anticyclones through narrow gaps (Simmons and Nof, 2001).

b. Earlier work

Eddy-island collisions were previously addressed by Stern (2000) who studied the scattering of barotropic eddies (advected toward a right cylinder by potential flow) using a contour dynamical method. His study concentrated on self-advection induced by perturbations to the eddy structure resulting from nondestructive collisions. He also presented an example of a contour which became multiply connected (i.e., eddy splitting) due to an intense collision. He did not, however, investigate this phenomenon quantitatively. Below we list a number of other investigations which address various components of the present problem, and hence are clear antecedents to our work.

The first investigation of CIAM for a rotating patch of fluid whose depth vanishes along its boundary is due to Ball (1963). This was extended by Nof (1990, 1991) to the more general case of a region with anomalous vorticity bounded by a vortex sheet, in which the depth along the boundary is neither zero nor necessarily constant. Cushman-Roisin (1989) examined the question of eddy *merging* by allowing for weak filaments and including

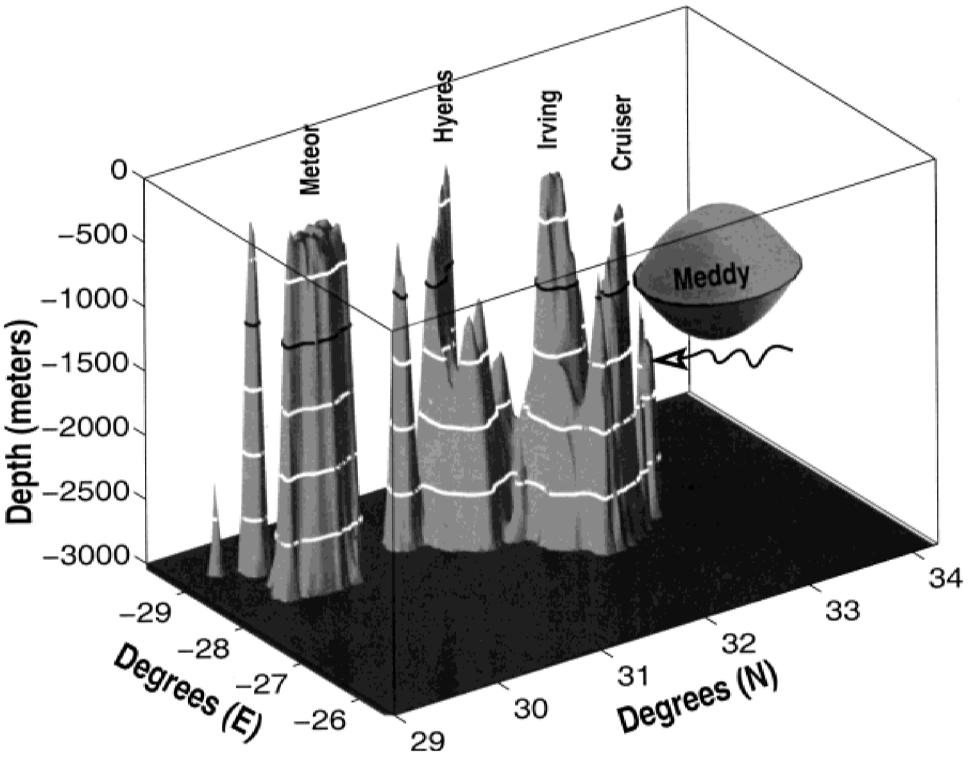

Figure 1. Perspective view of a collision of a Meddy with the Great Meteor Seamounts. The Meddy (indicated by the "UFO") structure is reconstructed in detail (i.e., thickness, size, and Rossby number) from data reported in Richardson and Tychensky (1998). Its diameter is 150 km, its central depth is −1100 meters, and its thickness is 1100 meters. (Note that this Meddy is one of the largest ever reported.) Richardson and Tychensky (1998) reported that the Meddy was split into two smaller offspring as a result of the collision. The "wiggly" arrow indicates the pre-collision southwestward migration of the Meddy. White lines are drawn on the seamounts at 500 meter intervals, and the 1100 meter depth contour is indicated as a black line along the rim of the Meddy and the seamounts. Topography below 3000 meters has been flattened for clarity. The seamounts (individually, and in ensemble) are $O(R_1)$ obstacles and thus are candidate Meddy splitters. From this point of view, we see that the seamounts are nearly vertical when compared to the horizontal scales of the Meddy and that their ensemble resembles a long thin wall. (One thirtieth degree topography data from the data set of Smith and Sandwell, 1997.)

angular momentum. Shi and Nof (1993) investigated an eddy which is forced violently into an infinite lateral boundary. They find that the collision strips off fluid from the rim of an eddy, leaving a core behind. While this is in some manner analogous to the splitting process which we shall discuss here, we must stress that we are not considering the impingement of an eddy against an infinitely long vertical wall, but rather a thin wall of finite length which cuts through the migrating eddy. Various aspects of eddy collisions with infinite vertical walls can also be found in Minato (1982, 1983), Yasuda *et al.* (1986), Masuda *et al.* (1987),

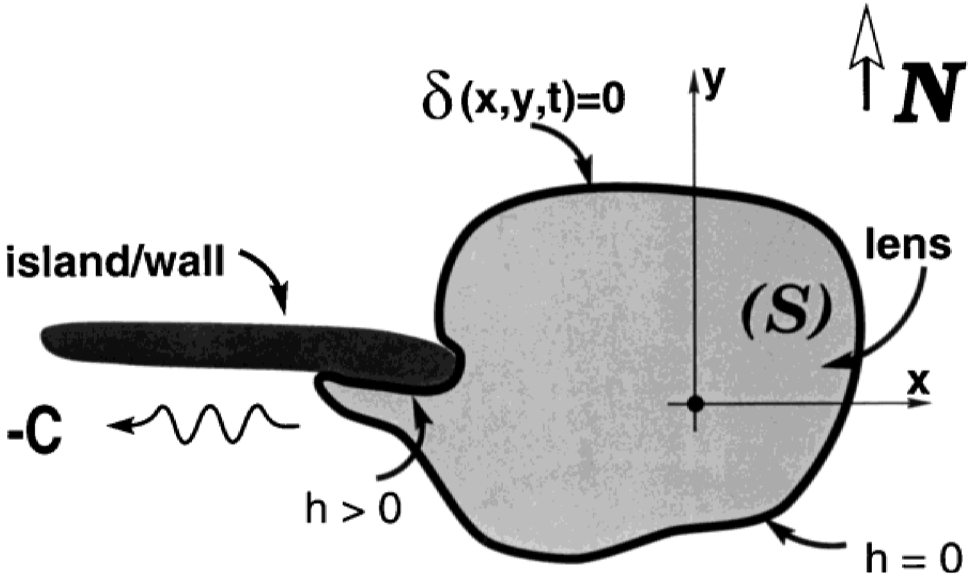

Figure 2. Schematic diagram of an isolated patch of fluid (i.e., a lens with a vanishing thickness along the off-wall edge) in contact with a wall (island). The shaded area occupied by the lens is **S**, the boundary is defined by a function $\delta(x, y, t) = 0$ (dark line), and the layer thickness is h. Along the wall, the fluid thickness is nonzero. The lens is migrating toward the island at a speed $-C$.

Umatani and Yamagata (1982), Masuda (1986), Nof (1988a,b; 1999), and Sanson *et al.* (1998). Finally, the reader is also referred to Louis *et al.* (1982), Smith and O'Brien (1983), Mory *et al.* (1987), Carnevale *et al.* (1991), Swaters and Flierl (1991), Velasco Fuentes and van Heijst (1994), Kamenkovich *et al.* (1996), and to LaCasce (1998), where the response of eddies to bottom topography is discussed.

c. This study

We will build on the work of Nof (1990), who showed that a lens cannot split on its own; an external torque, such as might be supplied by a wall, is necessary. The rather special case of a thin wall which pierces the lens allows us to go beyond the Nof (1990) conclusion and explicitly relate an outcome (i.e., the size and the location of offspring produce by a split) to the initial conditions (i.e., the size of the initial lens and the length of the wall).

To do so, we will consider a thin zonal wall piercing a zero PV lens. By assuming that the redistribution of mass that forms the offspring is accomplished by geostrophic wall-jets, we can explicitly determine the torque supplied by a wall (Section 2). We will show that the assumption that the jets are geostrophic is equivalent to assuming that the speed of the moving wall is slow compared to the orbital speed of the lens. The CIAM will allow us to relate the torque due to the wall to integrated angular momentum production. This enables us to derive the aforementioned relationship between the outcome and the initial conditions. It turns out, however, that this relationship does not result in a closed problem. That

is, although we can relate the outcome to the initial conditions, we do not know in advance the final location or the volume of the offspring; an additional constraint is necessary. Closure is accomplished by assuming that the resultant lenses are in contact with each other in the final state (i.e., they are "kissing"). This will allow us to determine the redistribution of mass from the parent lens to the offspring. The solution obtained in this way provides the desired critical wall length (L_{crit}) below which splitting may not occur.

Numerical experiments will confirm that the splitting of the parent lens into two offspring is accomplished by a geostrophic wall-jet that forms a second lens at the far end of the wall. Using Lagrangian floats, we find that the fluid nearest the center and rim of the second lens is derived from fluid near the rim of the parent lens. Water at an intermediate radius in the second lens is derived from fluid initially found at an intermediate radius in the parent lens. Collisions with very long thin walls result in lenses which are widely separated (not kissing). In this case, our analytical solution (which assumes kissing) gives a *lower bound* on the mass redistribution in the final state. Shorter (i.e., close to, but still longer than L_{crit}) walls result in lenses whose final configuration is better described by our kissing assumption, with a concomitant improvement of the agreement between the analytical and numerical results. The numerically determined critical length is close to, but slightly above, the analytical L_{crit}. Numerical investigation of weaker lenses and the effect of β produce similar results, although the numerically determined critical wall length is somewhat smaller.

d. Applications

Our analytical and numerical results will then be applied to observed collisions of Meddies with seamounts for which there have been several inferences of destruction or splitting. The work is, however, of broader interest from a fundamental theoretical point of view, because anticyclones seem to be ubiquitous and long-lived features in the ocean. Meddies have been observed to exist for several years and decay slowly while translating their heat and salt anomalies over thousands of kilometers (Armi *et al.,* 1989; Richardson and Tychensky, 1998). Our theory represents an important first contribution to our understanding of non-dissipative, non-radiative mechanisms for eddy destruction.

The paper is organized as follows. In Section 2, the CIAM constraint is derived. In Section 3 we discuss anticyclones in unbounded domains, where [following Nof (1990, 1991)] it is shown that anticyclonic lenses cannot split on their own (i.e., without an external agent). In Section 4, the torque due to a wall of finite extent (an "island") is considered, and a solution relating the lens splitting criteria to the wall length is obtained. In Section 5 we present numerical experiments using a primitive equations reduced gravity lens model. In Section 6 we use the numerical model to investigate weak lenses and the effect of β. In Section 7 we apply our theory to observations of the collision of Meddies with seamounts. The limitations of the analysis are discussed in Section 8, and a summary is given in Section 9.

2. Conservation of integrated angular momentum

Here, the known CIAM [Ball (1963), Cushman-Roisin (1989), Nof (1990, 1991)], is extended to include the β-plane approximation and a moving coordinate system. We adopt a lens model for our eddies (Fig. 2) so that, in the absence of islands or boundaries, the layer thickness is zero along the periphery.

To obtain the CIAM, we consider the equations governing an isolated patch of inviscid fluid overlying a quiescent lower layer,

$$\frac{\partial u}{\partial t} + u\frac{\partial u}{\partial x} + v\frac{\partial u}{\partial y} - fv + g'\frac{\partial h}{\partial x} = 0 \tag{1}$$

$$\frac{\partial v}{\partial t} + u\frac{\partial v}{\partial x} + v\frac{\partial v}{\partial y} + f(u + C) + g'\frac{\partial h}{\partial y} = 0 \tag{2}$$

$$\frac{\partial h}{\partial t} + \frac{\partial}{\partial x}(hu) + \frac{\partial}{\partial y}(hv) = 0. \tag{3}$$

Here, the Coriolis parameter is $f = f_0 + \beta y$, the reduced gravity is $g' = g\Delta\rho/\rho_0$, the Cartesian components are (x, y) and (u, v), the upper layer thickness is h, and the remaining notation is conventional. The coordinate system translates in the x-direction at a speed C. (For convenience the notation is defined both in the text and in the Appendix.) Following Nof (1990) [keeping track of the terms new to this investigation, β and C], we eventually obtain:

$$\frac{\mathrm{d}}{\mathrm{dt}}\overbrace{\iint_S h\left[xv - yu + f\frac{x^2 + y^2}{2}\right]\mathrm{d}\mathbf{S}}^{\mathrm{IAM}} - \frac{1}{2}g'\oint_\delta [yh^2\,\mathrm{dy} + xh^2\,\mathrm{dx}] - \beta\iint_S hv\frac{x^2 + y^2}{2}\mathrm{d}\mathbf{S} + C\iint_S fhx\,\mathrm{d}\mathbf{S} = 0. \tag{4}$$

Three comments should be made with regard to (4). The first term is the production of integrated angular momentum (IAM) comprised of an integral of h times the pointwise angular momentum. (The reader may be more familiar with the pointwise angular momentum in polar coordinates, $rv_\theta + fr^2/2$, where rv_θ is the relative angular momentum, $fr^2/2$ is the contribution due to the rotation of the coordinate system, and r measures the distance from the origin of the coordinate system.) The second integral is the wall torque (τ_h) which accounts for changes in the integrated angular momentum by pressure forces acting along the wall. In the absence of walls, this term would vanish. It would also vanish for features that are symmetrical with respect to x and y. Both the third and the fourth terms are new. The third term is the β-torque (τ_β); further discussion of this term and the final term describing angular momentum production due to the migration, C, is postponed until Section 3, where we speak about the IAM relative to an arbitrary axis.

3. Prohibition against splitting of anticyclones in unbounded domains

In this section we introduce our lens model and recapitulate the Nof (1990, 1991) argument that an anticyclone may not split on its own in an unbounded domain. We conclude with a derivation of the familiar westward drift rate of a lens due to the angular momentum produced by β. This provides new insight into the nature of the β-torque and the choice of our coordinate system.

For the type of lens under consideration here, the general undisturbed expression for azimuthal velocity and layer thickness is,

$$v_\theta(r, Ro) = -\frac{1}{2} Ro f_0 r, \qquad \text{and} \qquad h(r, Ro) = H_0 - \frac{f_0^2 r^2}{8g'}(2 - Ro)Ro, \tag{5}$$

where Ro is the lens Rossby number. A zero PV eddy ($Ro = 1$) on an f-plane has the structure $v_\theta = -\frac{1}{2} f_0 r$, $h = H_0 - (f_0^2 r^2/8g')$, so that the IAM about an *arbitrary* point is

$$\text{IAM} = \iint_S \frac{1}{2} h[f_0(r_0^2 + 2r_0 r\cos\theta + r^2) + r_0 v_\theta \cos\theta + r v_\theta]\, d\mathbf{S} = \frac{1}{2} f_0 r_0^2 V, \tag{6}$$

where V is the volume of the lens $[\pi f^2 R^4/(16g')]$, and r_0 is the distance of the eddy's center from the center of our coordinate system. We now note that the IAM of a zero PV lens is zero about its own center of rotation. (To see this, recall that its relative vorticity is $-f_0$, so that the lens is stationary with respect to a fixed, non-rotating coordinate system.)

Following Nof (1991), we can now demonstrate that splitting of anticyclones is prohibited in an unbounded domain (i.e., no walls). On an f-plane, with $C = 0$, (4) becomes

$$\frac{d}{dt}\iint_S h\left[r v_\theta + \frac{1}{2} f_0 r^2\right] d\mathbf{S} = 0. \tag{7}$$

Since the IAM must remain constant and it is zero initially (for $r_0 = 0$), it must vanish at all times. If the lens were to split into two offspring (of equal size, for simplicity) such as is illustrated in Figure 3, then the IAM would have to increase to $(\frac{1}{2}) f_0 R_f^2 V_0$, and (7) cannot be true. Therefore, the CIAM prohibits a lens from splitting in the absence of boundaries. The reader is referred to Nof (1991), where it is shown that only a *cyclone* possesses the necessary initial IAM to split (since it rotates in the same sense as f). It is easy to show that energy *must* be lost during eddy fission because energy is proportional to H^3 (where H is the thickness at the center), whereas the volume is proportional to H^2. As in other idealized adjustment problems in inviscid systems, this loss can be accomplished by Poincaré waves.

Finally, it is worth mentioning that the free westward drift can be obtained from (4) by substituting the approximate values for h and v. For a zero PV lens, we get $(d/dt)(r_0) = -C - (\frac{2}{3})\beta R_d^2$. Following the center of the lens (i.e., setting $(d/dt)r_0 = 0$), we find that the lens propagates to the west at $C = -(\frac{2}{3})\beta R_d^2$, a result identical to that of Nof (1981) and Killworth (1983). Since the perturbations to the lens' structure due to β are weak (Nof, 1981), β can only appreciably change the angular momentum of a lens by inducing a

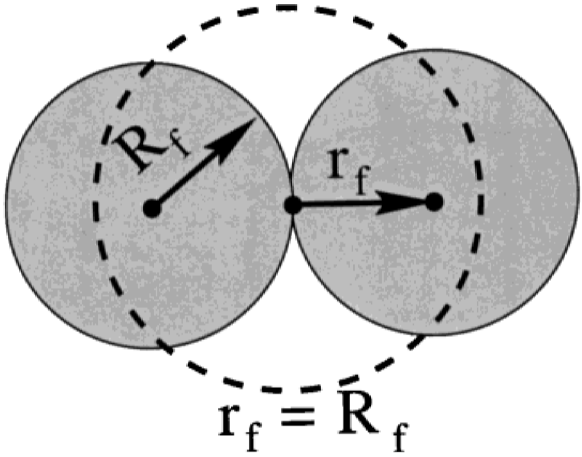

Figure 3. Configuration of a hypothetical lens splitting on its own (i.e., without a wall) into two lenses of equal size. The dashed line indicates the parent lens' position. We define the initial, unsplit lens as the "parent" and the final lenses as the "offspring." For simplicity, the edges of the offspring are taken to be tangential to the origin, so that the distance from the center of the coordinate system to the centers of the offspring, r_f, is equal to their radii, R_f. It is pointed out in the text that such a splitting cannot occur without an external source of angular momentum (such as a wall).

precession of the lens relative to the earth. By choosing a moving coordinate system such that the lens appears to be stationary, β produces no torque. Therefore, β *alone cannot break or significantly distort a lens* but can merely induce a translation.

4. Application of the integrated angular momentum to a splitting lens

By explicitly considering the wall torque in (4), we can connect the initial and final states for a lens that is split by a finite length wall. Specifically, we consider the analytically tractable case of a lens that is advected by a uniform barotropic flow into a thin wall oriented parallel to the advecting flow (Fig. 4a or 4b), and argue that this is identical to the case of a stationary lens and a translating wall. This kind of equivalence is obvious in the nonrotating case ($f \equiv 0$) but is not so obvious in the case when f is not zero because of the additional Coriolis force and the resulting modified version of the Bernoulli integral [$\frac{1}{2}(u^2 + v^2) + g'h + fCy =$ constant along a streamline] that involves an extra pressure term fCy.

To see this, consider again (2), the v-momentum for a coordinate system translating with the wall at a speed C toward a stationary lens. It turns out that this equation is identical to the v-momentum equation (in a fixed coordinate system), describing a lens advected by a uniform (geostrophic) lower layer flow $-C$ toward the thin wall. In the first of these two equations, the term Cf arises because of the apparent force due to the linear translation relative to a rotating coordinate system. In the second, the term Cf arises because of the

pressure force due to the sloping interface. Because the wall is very thin, the two v-momentum equations are equivalent, implying that the lens structure is unchanged by the lower-layer advection. This analogy is also reflected in the extra term in the Bernoulli integral, $fC\Delta y$ (where Δy measures the thickness of the wall), which is zero for a thin wall. Thus, without loss of generality, we can set $C = 0$ and have the wall moving toward the lens instead of the lens moving toward the wall.

a. Assumptions and derivations

We begin with a description of the slow splitting process forced by a wall moving slowly into the eddy (Fig. 4a or 4b). This description is based on both general principles and the numerical experiments described later in Section 5. We denote the parent lens as lens 1, and the offspring as lenses 2 and 3. First, the wall pierces the parent lens (Fig. 4, panel 1) and the anticyclonic flow along the rim stagnates somewhere. Subsequently, the flow bifurcates at the tip of the wall, with part of the flow continuing to circulate within the parent lens, and the other part forming a wall-jet which flows along the wall in the Kelvin wave sense (Fig. 4, panel 2). When this jet reaches the end of the wall (Fig. 4, panel 3), it turns back on itself in order to return along the opposite portion of the wall. At the expense of the shrinking parent lens, the retroflecting jet must now form a second lens (lens 2) so that the momentum flux of the jets is balanced (Pichevin and Nof, 1996). When the moving wall completes its passage through the lens, the parent has been split into two offspring (Fig. 4, panel 4).

With $\beta \equiv C \equiv 0$ and the one-dimensionality of the wall, the CIAM (4) takes the simplified form,

$$\frac{\mathrm{d}}{\mathrm{dt}} \iint_{\mathrm{s}} h\left[rv_\theta + \frac{1}{2} f_0 r^2\right] \mathrm{d}\mathbf{S} = \frac{1}{2} g' \oint_{\delta} xh^2 \, \mathrm{dx}. \tag{8}$$

To apply (8) to our splitting process, we shall integrate in time so that we shall be able to connect the initial and final states.

i. Scales. Attending first to the right-hand side, we assume that at all times, h^2 is approximately uniform along *each* side of the wall so that h^2 is independent of x and can be taken outside of the line x-integral. This assumption is equivalent to the geostrophic approximation for the jet because it implies that the geostrophic transport $[g'h^2/(2f)]$ is approximately constant along the wall. It also means that disturbances propagate very quickly along the wall. This does not imply, however, that h does not vary in time. Specifically, we neglect the variations of h in x but not in time, which, though small, accumulate during the process to become important.

Note that when the fluid depths are identical on the two sides of the wall, the integrand vanishes. (This cannot be the case with our splitting lens.) Also, note that the jet's "nose" is ageostrophic during the time that it runs down the wall. We assume that this ageostrophic portion of the drainage contributes negligibly to the total accumulated torque because of its

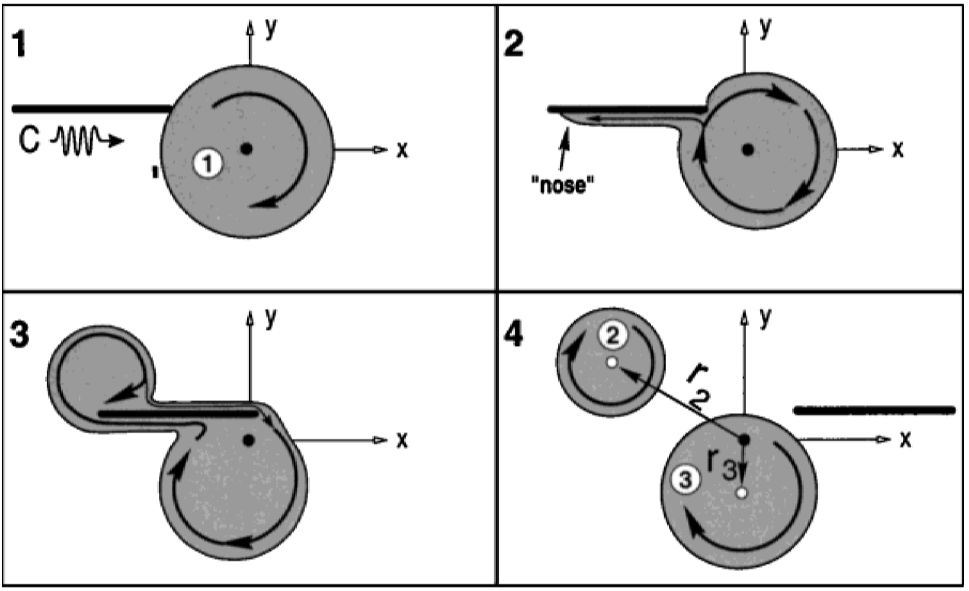

Figure 4(a). A typical lens splitting process due to a moving wall (with time progressing clockwise from 1–4). The "wiggly" arrow denotes the moving wall speed. The "parent" lens is the initial lens (lens 1 in panel 1), whereas the "offspring" are the resultant lenses (lenses 2 and 3 in panel 4). Note that lens 3 is the reduced core of lens 1. The coordinate system is attached to the initial center of the parent lens, indicated by the black dot in each frame. In panel 1, the moving wall is just "kissing" the lens. In panel 2, the flow around the rim stagnates and splits, and some of the fluid runs along the wall as a wall-jet. As shown in panel 3, when the jet reaches the end of the wall, it retroflects and develops a second lens (see Pichevin and Nof, 1996). Finally, the wall has completed its passage through the parent lens, which, as a result, has split into two children (panel 4). The parameters r_2 and r_3 (indicated by the open circles) define the offsprings' centers of rotation in the *final,* split configuration. Note that r_2 and r_3 are not time dependent. This configuration is based on both our understanding of the problem and the numerical experiments discussed later in Section 5; it will later be referred to as "mode 1."

small size relative to the wall length. This again implies that the time that the drainage takes to be set up (T_{jet}) must be small compared to the total time of the encounter (T_{enc}).

The timescale of the encounter is scaled by the wall length (L) and the migration of the wall (C), i.e., $T_{\text{enc}} \sim O(L/C)$. The application of the Bernoulli integral implies that the speed of the jet's nose (U_{jet}) should be of the same order as the speed along the rim of the lens. Thus $U_{\text{jet}} \sim O(g'H_1)^{1/2}$, where H_1 is the central thickness of the parent lens, and $T_{\text{jet}} \sim O(L/U_{\text{jet}})$. We now define a small parameter $\varepsilon = C/(g'H_1)^{1/2} \ll 1$. Our neglect of ageostrophic contributions to the integral is, therefore, justified as long as

$$\varepsilon = \frac{C}{U_{\text{jet}}} \ll 1. \tag{9}$$

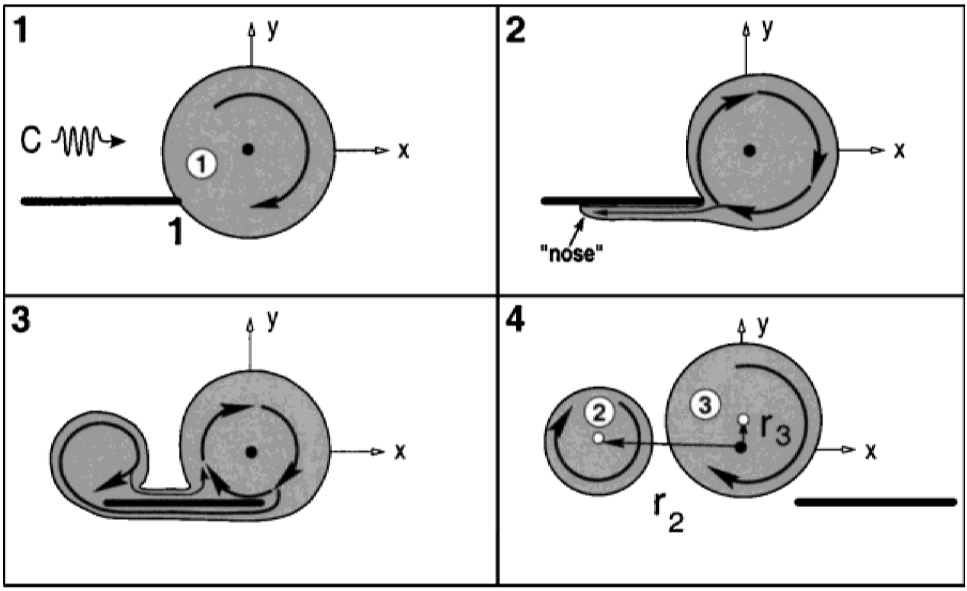

Figure 4(b). As in Figure 4(a), but for what will be later referred to as "mode 2." (Again, based on our understanding of the problem and the numerical experiments discussed in Section 5.)

Thus, the speed at which the wall is driven into the lens must be slow compared to the swirl speed of the lens. It should also be pointed out that, at the point where the jet retroflects, there may be a small region where there is separation of the streamline from the wall (Nof and Pichevin, 1996). However, this can only occur over such a small region that it has a negligible effect on the total accumulated torque.

Before proceeding to derive our solution, we can demonstrate [via a scaling of (8)] that the wall length required to split a lens must be $O(R_1)$ in all cases, even when the wall is merely brushing the parent lens. To see this, we begin by noting that, for splitting a lens, the balance in (8) can be written as,

$$f_0 R_1^2 V \sim O(T_{\text{enc}} g' h_w^2 L^2). \tag{10}$$

The left-hand side is the final IAM for a zero PV lens, given by (6). Here, the radius of the offspring is scaled by R_1 (the radius of the parent lens) and the offspring's volume, V, is scaled by the volume of the parent lens. The thickness scale, h_w, is the thickness of the fluid along the wall during the collision. Since the redistribution of mass occurs via geostrophic wall-jets, we can also scale V by the time integral of the geostrophic transport along the wall,

$$V \sim O\left(T_{\text{enc}} \frac{g' h_w^2}{f_0}\right). \tag{11}$$

Combining (10) and (11) we get,

$$f_0\left(T_{\text{enc}}\frac{g'h_w^2}{f_0}\right)R_1^2 \sim O\,(T_{\text{enc}}g'h_w^2L^2),$$

implying that, as stated above, L is $O\,(R_1)$ for all cases.

We shall now calculate the scale for h_w. The volume of a zero potential vorticity lens is $4\pi g'H^2/f^2$ so that,

$$V \sim O\left(\frac{g'H_1^2}{f^2}\right) \sim O\left(\frac{T_{\text{enc}}g'h_w^2}{f}\right),$$

implying that $h_w \sim H_1/(T_{\text{enc}}f)^{1/2}$. Since L is $O\,(R_1)$, it follows that $T_{\text{jet}} \sim O\,(f^{-1})$, and, therefore, $\varepsilon \sim O\,(fL/C)$. Together with the estimate for h_w just mentioned, this implies that $h_w \sim O\,(\varepsilon^{1/2}H_1)$. In summary, our scales are, $\varepsilon = C/(g'H_1)^{1/2} \ll 1$, $L/R_1 \sim O\,(1)$, and $h_w \sim O\,(\varepsilon^{1/2}H_1)$.

Recall that the above scaling for h_w applies only to a split in which the offspring are $O\,(V)$ in the final state. If we were to apply our scaling to the case of a very weak split (where the volume of lens 2 is a very small fraction of the total volume of fluid) then the proper scaling for h_w would be $h_w \sim O\,(\varepsilon^{1/2}H_2)$, where H_2 is the central depth of lens 2, (as defined by Fig. 4) instead of $\sim O\,(\varepsilon^{1/2}H_1)$. By repeating the procedure we just performed, it is easy to show that the scaling for L remains $L/R_1 \sim O\,(1)$. We shall see later that all of these scales are in agreement with the numerics.

ii. Simplified equations. We shall now derive the algebraic equations resulting from the simplified integrated angular momentum constraint. By integrating the right-hand side of (8) around the wall, we get,

$$\frac{\mathrm{d}}{\mathrm{d}t}\iint_{\mathrm{S}} h\left[rv_\theta + f_0\frac{r^2}{2}\right]\mathrm{d}\mathbf{S} = \frac{g'}{4}\Delta h_w^2L^2, \tag{12}$$

where Δh_w^2 is the difference between h_w^2 across the wall. Recall that, for all times, h_w is assumed to be approximately constant along each side of the wall (but not necessarily the same along the two opposite sides of the wall). Integrating once in time from the initial, un-split state to the final split state (when the wall has completed its passage) we get,

$$\iint_{\mathrm{S}} h\left[rv_\theta + f_0\frac{r^2}{2}\right]\mathrm{d}\mathbf{S} = \frac{g'}{4}L^2\int_0^T \Delta h_w^2\,\mathrm{d}t, \tag{13}$$

where T is the time interval connecting the initial and final states and, as stated earlier, h_w varies in time. [Recall that, even though h_w varies slowly in time, the changes in h_w accumulate over a long time to become important.] For a PV conserving process resulting in two lenses we can use (6) to evaluate the left-hand side of (13) at the final state. Recall

that, as discussed in Section 3, the IAM is zero in the initial state. With this evaluation, (13) takes the form,

$$\frac{1}{2} f_0(r_2^2 V_2 + r_3^2 V_3) = \frac{g'}{4} L^2 \int_0^T \Delta h_w^2 \, \mathrm{dt}. \tag{14}$$

The subscripts 2 and 3 label the offspring (as defined in Fig. 4); r_2 and r_3 are the distances from the center of the parent lens to the centers of the offspring, and V_2 and V_3 are their volumes.

We now define γ, the ratio of the volumes,

$$\gamma = V_2/V_3, \tag{15}$$

and point out that V_2, as defined in Figure 4, is always in the numerator, so that in principle, γ can range from zero to infinity. We can then rewrite (14) as

$$\frac{1}{2} f_0 V_2 \left(r_2^2 + \frac{1}{\gamma} r_3^2 \right) = \frac{g'}{4} L^2 \int_0^T \Delta h_w^2 \, \mathrm{dt}, \tag{16}$$

and note that the net geostrophic mass flux into lens 2, due to the difference between the flux from the wall jet adding mass to lens 2 and any (smaller) jet on the opposite side removing mass, is $Q = g' \Delta h_w^2/(2f_0)$ for all times. Thus we can derive a second equation for V_2 by integrating Q over the time of the encounter,

$$\int_0^T Q \, \mathrm{dt} = V_2 = \frac{g'}{2f_0} \int_0^T \Delta h_w^2 \, \mathrm{dt}. \tag{17}$$

The time integral in (16) and (17) need not be specifically evaluated and a substitution of (17) into (16) gives us the final form of the integrated angular momentum,

$$\boxed{r_2^2 + \frac{1}{\gamma} r_3^2 = L^2.} \tag{18}$$

This equation, originally derived from (4), relates the final locations and volumes of the offspring (r_2, r_3) to the wall length L. Before proceeding, it is useful to point out again that the assumptions that we used to derive (18) are: (i) the lenses have zero PV, (ii) the time associated with the establishment of the jets is rapid compared to the total time of the encounter so that the problem is a slowly varying process, (iii) during the slowly varying encounter the flow along the wall is geostrophic, and (iv) separation of the flow at the tip of the walls is unimportant.

b. General solution

To determine the outcome of the slow collision between the wall and the lens we will, of course, use the conservation of mass. Conservation of PV is implicit because we already assumed that the structure at the beginning and end state is that of the zero PV lens. Since

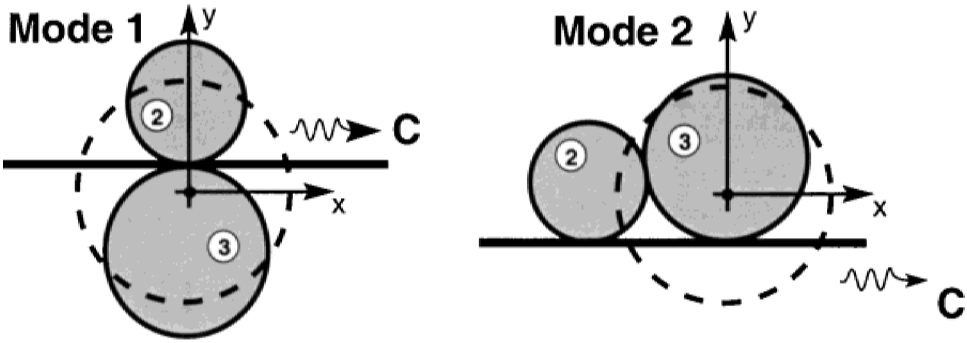

Figure 5. Schematic diagram of two idealized "modes" for the final state of a lens split by a slowly moving wall. The modes are based on both our understanding of the problem and the numerical experiments discussed later in Section 5 and shown earlier in Figure 4. The location of the "parent" lens is indicated with the dashed circle in the background, and the "offspring" are shown in the foreground. The path that the wall travels is indicated with the dark straight line. The wall travels slowly at a speed C, indicated by the "wiggly" arrow. In both modes, the offspring are tangential to the axis of the wall. In mode 1, the offspring are on opposite sides of the wall, whereas in mode 2 they are on the same side of the wall. The detailed geometry and variables used to determine the wall lengths capable of splitting a lens can be found in Figure 6. Mode 1 will be realized when the "contact point" (i.e., the point where the wall impinges on the lens) is "above" the center of the parent lens, whereas mode 2 will be realized when the initial contact point is "below" the center. The precise location of the transition will be determined by our numerical experiments.

we do not know in advance where the lenses end up, nor do we know the partitioning of mass between the children, the variables r_2, r_3 and γ are free parameters. It is easy to see that with our approach of connecting the initial and final states, our problem requires a closure condition. This will be provided in the form of an assumed final geometry (later supported by our numerics).

As shown in Figure 5, we pose two possible final configurations ("modes") that are based on both our physical understanding of the problem and the numerical experiments presented later in Section 5. The region of applicability of each of the two modes will be determined by our numerical experiment. For both modes, the assumptions are: (a) the final lenses are tangential to the axis of the wall, (b) during the encounter, lens 3 experiences displacement only in the y-direction, and (c) the final lenses are minimally separated, i.e., the offspring are "kissing" each other. We will now discuss the detailed solutions for each of the modes.

c. Detailed solution: Mode 1

i. Geometry. The geometry shown in Figure 6 implies that,

$$r_2 = d + R_2 \tag{19}$$

and

$$r_3 = R_3 - d. \tag{20}$$

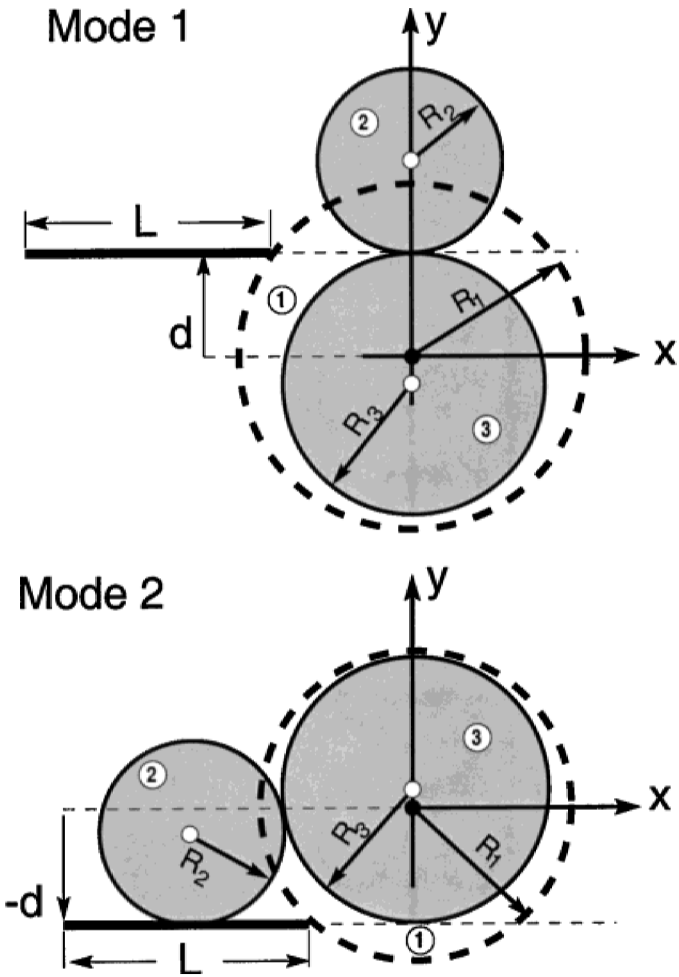

Figure 6. Definition of variables for modes 1 and 2. We seek a final, split state obeying the constraints: (a) the final eddies are kissing each other, (b) the eddies are tangential to the original axis of the wall, and (c) the reduced parent lens experiences negligible displacement in the x-direction. The length of the wall is L. The distance (in the y-direction) from the origin of the coordinate system (defined by the center of the parent lens and indicated by the axes) to the initial contact point between the lens and the wall is d. The variables R_1, R_2, and R_3 are the radii of the parent (lens 1) and the offspring lenses (lenses 2 and 3). The centers of the offspring are indicated by the white circles.

We now note that, for a zero PV lens, conservation of mass requires that

$$R_2^4 + R_3^4 = R_1^4. \tag{21}$$

This completes the derivation of the conditions imposed by our chosen geometry.

ii. Known and unknown variables. We now have five algebraic equations [(15), (18), (19), (20), and (21)], with seven variables (L; R_2; R_3; r_2; r_3; γ; d). Out of the seven variables, two

variables are known (L; d), so that our problem is closed (i.e., we have five equations with five unknowns). Using (19) and (20) to eliminate r_2 and r_3 from (18), we obtain

$$(d + R_2)^2 + \frac{1}{\gamma}(R_3 - d)^2 = L^2. \tag{22}$$

Using (21) and (15), we can write R_2 and R_3 in terms of γ:

$$R_2^4 = \frac{\gamma}{\gamma + 1} R_1^4 \qquad \text{and} \qquad R_3^4 = \frac{1}{\gamma + 1} R_1^4, \tag{23}$$

and (22) finally becomes,

$$L^2 = \left[d + R_1\left(\frac{\gamma}{\gamma + 1}\right)^{1/4}\right]^2 + \frac{1}{\gamma}\left[d - R_1\left(\frac{1}{\gamma + 1}\right)^{1/4}\right]^2. \tag{24}$$

Eq. (24) is an implicit equation for γ (the single unknown variable describing the final state) in terms of the two knowns (L, d). It is difficult to write an explicit expression for γ in terms of L and d, but this is not essential as we can numerically evaluate (24) to tabulate (L, a, γ) and, using (19), (20), and (23), show the solution for (R_2; R_3; r_2; r_3; γ) as a function of d (Fig. 7, panels 1–5).

d. Detailed solution: Mode 2

For mode 2 (Fig. 5), the analogous geometric constraints (Fig. 6) are $r_3 = R_3 + d$, and $r_2 = [4R_2R_3 + (d - R_2)^2]^{1/2}$. We ultimately find that

$$L^2 = 4R_1^2\left(\frac{\gamma}{\gamma + 1}\right)^{1/4}\left(\frac{1}{\gamma + 1}\right)^{1/4} + \left[d - R_1\left(\frac{\gamma}{\gamma + 1}\right)^{1/4}\right]^2 + \frac{1}{\gamma}\left[R_1\left(\frac{1}{\gamma + 1}\right)^{1/4} + d\right]^2. \tag{25}$$

The solutions for (R_2; R_3; r_2; r_3; γ) as a function of d are now shown in panels 1–5 of Figure 8. These were obtained in a similar manner to those of mode 1.

e. Implications of our analytical solution

i. Multi-valued outcomes. One important feature of our solution is that for each mode, some outcomes are multi-valued. That is, for a given set of initial conditions, (L, d), more than one outcome (R_2; R_3; r_2; r_3, or γ) appears to be possible. This means that, in order to determine the solution for a given L and d, we not only need to *a priori* select one out of the two modes, but we also need to decide on a single solution for each mode. The multi-valued aspect is particularly evident in panel 6 of Figures 7 and 8, where we have plotted L as a function of d for various values of γ; where the curves intersect, the solution is multi-valued. We can select a single-valued physically relevant solution by adopting the following logic. Since larger values of γ represent greater drainage from the parent lens, we expect that the offspring lenses attain (and remain at) the first viable solution (i.e., the lower value of γ). That is, although other values of γ may be physically realizable, we reject them

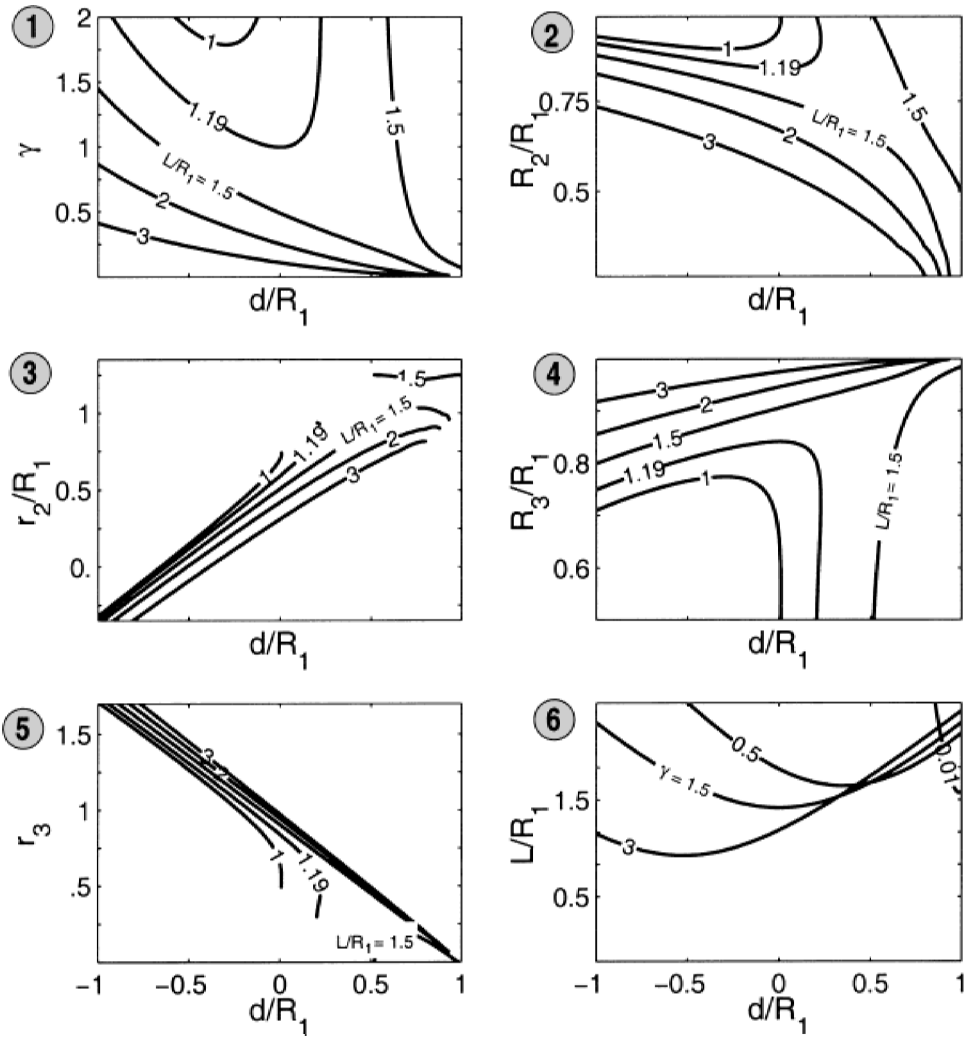

Figure 7. Analytical solutions for mode 1 [according to (24)]. The first five panels show the five variables, R_2; R_3; r_2; r_3; γ as a function of d (for various values of L). The sixth panel represents an inversion of the solution and shows L as a function of d for various values of γ. Our solution is multivalued above $d/R_1 \approx 0.3$, as is clearly evidenced by the intersection of the lines of constant γ in panel 6. It is argued in the text that only the branches corresponding to the smaller value of γ will be physically realized.

on the grounds that they will not be reached. Our numerical simulations suggest that this is indeed the case.

ii. Separation of the modes. While determining the nature of the separation between the two modes would likely require solving the incredibly complicated time dependent

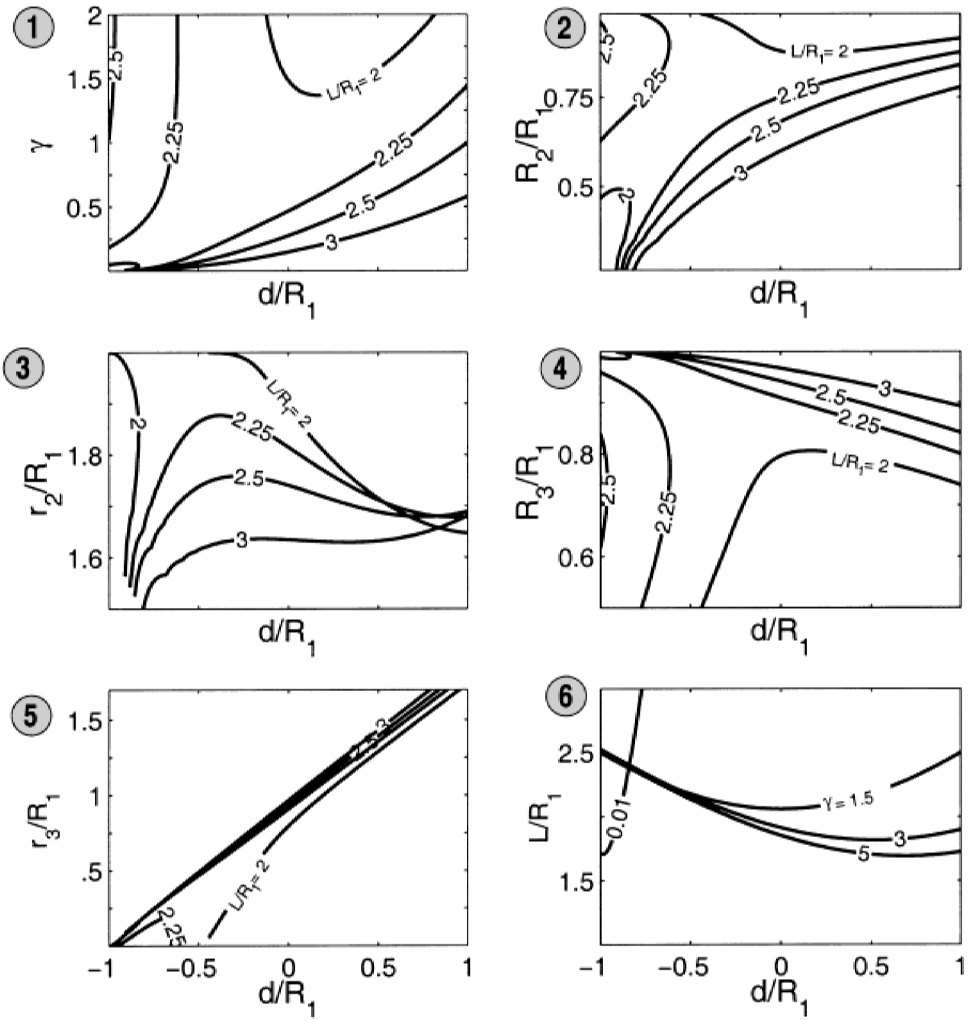

Figure 8. Analytical solutions for mode 2 [according to (25)]. The first five panels show the five variables, R_2; R_3; r_2; r_3; γ as a function of d (for various values of L). The sixth panel represents an inversion of the solution and shows L as a function of d for various values of γ. As in mode 1, the solution is multivalued below $d/R_1 \approx -0.5$. (This is clearly evidenced by intersection of the lines of constant γ.)

problem (which is beyond the scope of this study), it is easy to understand why the separation between the modes occurs for $d < 0$. As the fluid forms lens 2, there is momentum flux out of the parent lens, directed in the negative x-direction. Consequently, the lens must translate in the negative y-direction so that a compensating integrated Coriolis force (associated with the lens' migration) is established. When $d = 0$, the lens' center must shift away from the wall in the negative y-direction and we end up with a mode

1 outcome (i.e., lens 3 shifts "below" the wall). When $d/R_1 \to -1$, only a very small amount of fluid can leak along the wall, and as a result, an $O(R_1)$ shift in the negative y-direction is neither required nor possible. Hence, a mode 2 outcome must result (i.e., lens 3 remains "above" the wall). Clearly, the separation between the modes must be at some value of $d < 0$. Our numerical simulations (Section 5) show that it occurs at $d/R_1 \approx -0.45$.

iii. Weak collisions. In light of our scaling which showed that, in order for a wall to induce a split, L must always be $O(R_1)$, it is appropriate to examine our solution in the limit of weak collisions (i.e., the wall is close to the lens' edge corresponding to $d/R_1 \to \pm 1$ and $\gamma \to 0$). Recall that for $d/R_1 \to 1$ and $\gamma \to 0$, one may (erroneously) expect that $L \to 0$ (i.e., one might expect that a short wall will be sufficient to split off a small portion of the parent lens). In line with our earlier scaling, we find that, in this limit, (24) becomes $L/R_1 = 1$ as should be the case (see panel 1, Fig. 7). Similarly, as $d/R_1 \to -1$, $\gamma \to 0$, and, again $L/R_1 \to 1$ (panel 1, Fig. 8).

5. Numerical experiments

In this section we compare our theory with numerical simulations which explicitly include (albeit approximately) the time dependent processes circumvented in the analytical solution. We first give the model description and configuration, and then describe the splitting process. This is followed by our comparison with the analytical solution, and comparisons with the CIAM at various levels of simplification. Later on we shall discuss a lower bound on the wall length capable of splitting a lens.

a. Model description and configuration

Numerical experiments were conducted using a finite difference (C-grid), primitive equation, reduced gravity numerical model derived from that of Bleck and Boudra (1986), which integrates (1)–(3) [with $C \equiv 0$, and the introduction of Laplacian friction]. This type of model is especially well suited to studies of lenses because of its flux-corrected transport advection algorithm (Zalesak, 1979) that performs well in regions of discontinuities (as are present at the boundary of a lens). We conducted three sets of numerical experiments (Table 1). Set 1 was specifically designed to test our theory (using a stationary zero PV lens and a moving wall) and is discussed in this Section. Sets 2 and 3 correspond to extensions of our theory and are discussed in Section 6. The basic strategy for all the experiments was to alternately vary the wall length (L) and the initial contact point between the wall and the lens (d).

On a C-grid, the wall is defined as a set of no-flux boundary conditions on v-points. The wall was driven into the lens by shifting the no-flux boundary conditions by one full grid point each model day (≈ 9 cm s^{-1}). For the zero PV lens model employed here, this corresponds to $\varepsilon = C/(g'H_1)^{1/2} = 0.03$. Splitting is said to have occurred when two distinctly different closed contours (defined by $h/H_1 = 0.2$) appear, and when the two

Table 1. Parameters for the three sets of numerical experiments. In the first column we give the set number (composed of a group of experiments with a unifying physics, but differing geometries) and in the second we give the experiment number. In the third we give the Rossby number of the lens ($R_o = 1$ corresponds to a zero PV lens), in the fourth the initial lens thickness, in the fifth the value of β, in the sixth the value of the Laplacian friction coefficient, and in the seventh the horizontal grid spacing. For all experiments, the reduced gravity was 0.986 cm s^{-2}, the initial eddy radius was 144 km, and the Coriolis parameter was 5×10^{-5} s^{-1}. Set 1 is designed to test our theory (i.e., it explores the splitting of a zero PV lens pierced by a moving wall). In set 2, we explore the differences arising from a weak ($R_o = 1/4$) lens, whereas in set 3 we explore the splitting of a zero PV lens driven by β into a stationary wall.

Set	Experiment #	*Ro*	H_1 (m)	β (cm^{-1} s^{-1})	A_H	Δx
1	1–132	1	600	0	4×10^6 cm^2 s^{-1}	8 km
1	133–134	1	600	0	2×10^6 cm^2 s^{-1}	4 km
2	135–266	1/4	150	0	4×10^6 cm^2 s^{-1}	8 km
2	267–269	1/4	150	0	2×10^6 cm^2 s^{-1}	4 km
3	270–318	1	600	6.0×10^{-13}	4×10^6 cm^2 s^{-1}	8 km

lenses defined in this manner persist for more than ten revolutions (thirty days). The choice of $h/H_1 = 0.2$ was consistent with the requirement that the lenses remain distinct for at least ten revolutions without re-merging. We found that the lenses rapidly coalesce when the minimum fluid thickness separating the lenses exceeded the above amount. Determination of the volume necessary for the computation of γ is achieved by examining the volume of fluid enclosed by the contour $h/H_1 = 0.2$. Mass is only conserved to within about 70% by our definition of lens boundary, but this has no bearing on our analysis. [Mass is conserved to machine precision over the whole domain.]

b. Set 1: A test of Eqs. 24 and 25

To validate the theory, 132 individual experiments were performed with d taking on 11 evenly distributed values from −120 km to 120 km ($-0.9R_1$ to $0.9R_1$) and L taking on 12 evenly distributed values from 144 km to 408 km ($1.0R_1$ to $2.9R_1$). Figure 9 is a graphical summary of the outcome of all 132 experiments run at 8 km grid resolution. [Three additional resolution doubling experiments were conducted at $d = 0$, and $L = 1.6R_1$, $1.5R_1$, and $1.4R_1$.]

i. Brief description of the splitting process. Splitting unfolds much as was shown earlier in Figure 4. Generally speaking, we find that long walls produce splitting with offspring that are widely separated from each other. As the wall length is reduced, the lenses are proportionately closer to each other in their final configuration (Fig. 10, panel 5). Below a critical wall length, splitting does not occur (Fig. 11). (Detailed discussion of this critical wall length is postponed until Section 5(b)v.)

Figure 12 reveals that lens 2 is derived of fluid which is stripped from the outer portion of the parent lens. It is also clear that lens 2 is built up in such a way that its core is derived

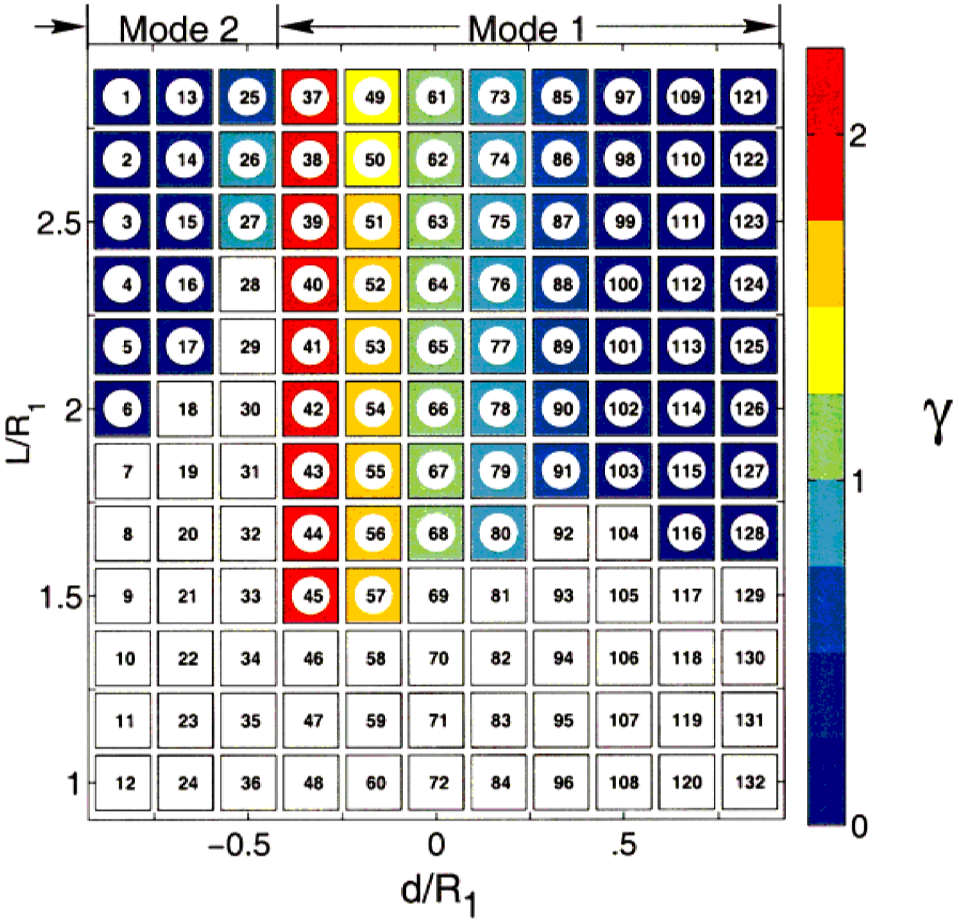

Figure 9. Summary of the experiments of set 1 (experiment number is indicated in each square). The color code indicates the value of γ. White indicates experiments where no splitting occurred. Note that γ does not vary much with L. Also note that there is a critical value (L_{crit}), below which splitting does not occur. The jump between modes 1 and 2 is at $d/R_1 = -0.45$, and is visible as a jump in both γ and L_{crit} (e.g., from experiment 27 to 45).

from fluid originating from the rim of the parent lens ($r/R_1 \rightarrow 1$). The general structure of the second lens can be understood by considering the analogy with winding thread from a full to an empty spool. As the fluid (thread) which is initially at the perimeter of the first lens (spool of thread) drains (unwinds), it forms the core of the second lens (accumulating spool). Thus the radial distance of the fluid in the second lens is reversed from its position in the parent. In detail the process is somewhat more complicated because as lens 2 grows due to the influx of fluid from the parent lens along one side of the wall, it is also losing some (smaller) amount of fluid by a return flow back to the parent along the opposite side

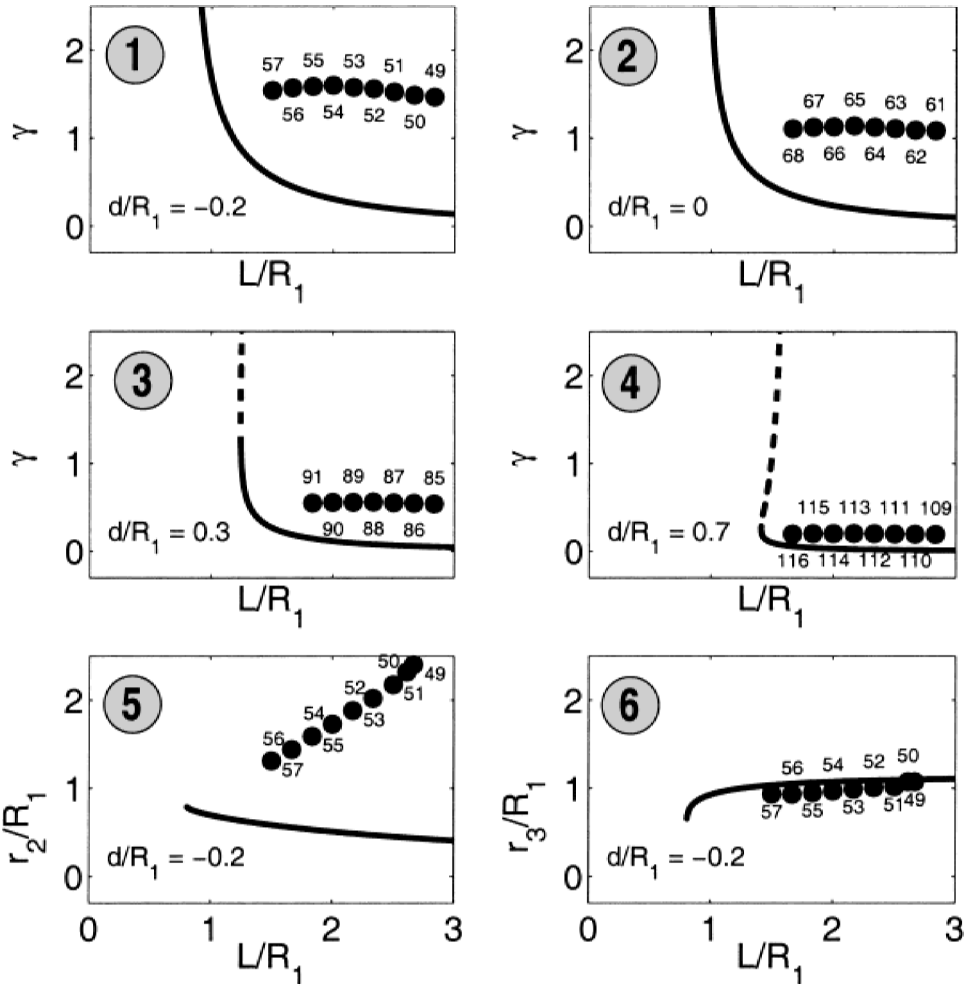

Figure 10. Comparison between the numerical and the analytical γ as a function of L for various values of d for mode 1 (panels 1–4). Numerical experiments are shown as solid circles and theoretical solutions are indicated as lines. The bottom two panels show r_2 as a function of γ and r_3 as a function of γ. Experiment numbers (from set 1) are labeled next to their respective circles. The dashed lines indicate the branches where a multivalued solution is rejected on the grounds that it cannot be reached. The theory clearly gives a lower bound on the mass redistribution, γ, that occurs as a result of a collision with a wall (panels 1–4). It also gives a lower bound on the location of the second lens, (r_2, shown in panel 5), and an upper bound on the position of the reduced core of the parent lens, (r_3 shown in panel 6). The worst agreement between the analytics and numerics is in the determination of r_2 (panel 5), which is quite sensitive to our (somewhat artificial) closure condition. This agreement is substantially improved as the wall length is shortened because, for shorter walls, the separation between the offspring is reduced (e.g., experiments 49 vs 57).

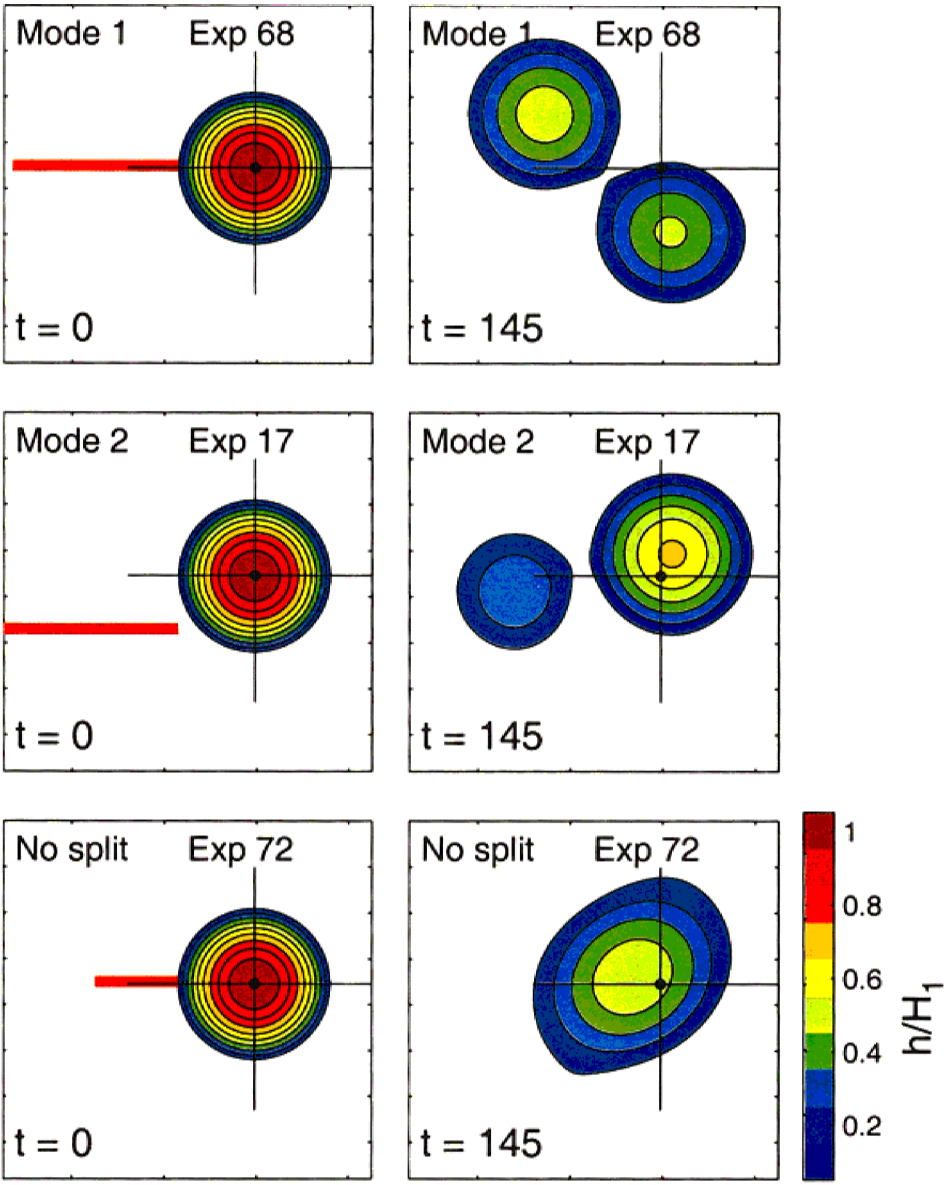

Figure 11. Typical numerical splitting of a lens by a collision with a wall (set 1). In the top (central) panels, we show a wall that is longer than the critical length which can result in a split of mode 1 (2). In the bottom panels we show a wall that is shorter than the critical length and, consequently, no splitting occurs. Note that there has been very little displacement in the *x*-direction of lens 3 (defined in Fig. 4). Axes defining the origin of the coordinate system are shown for reference.

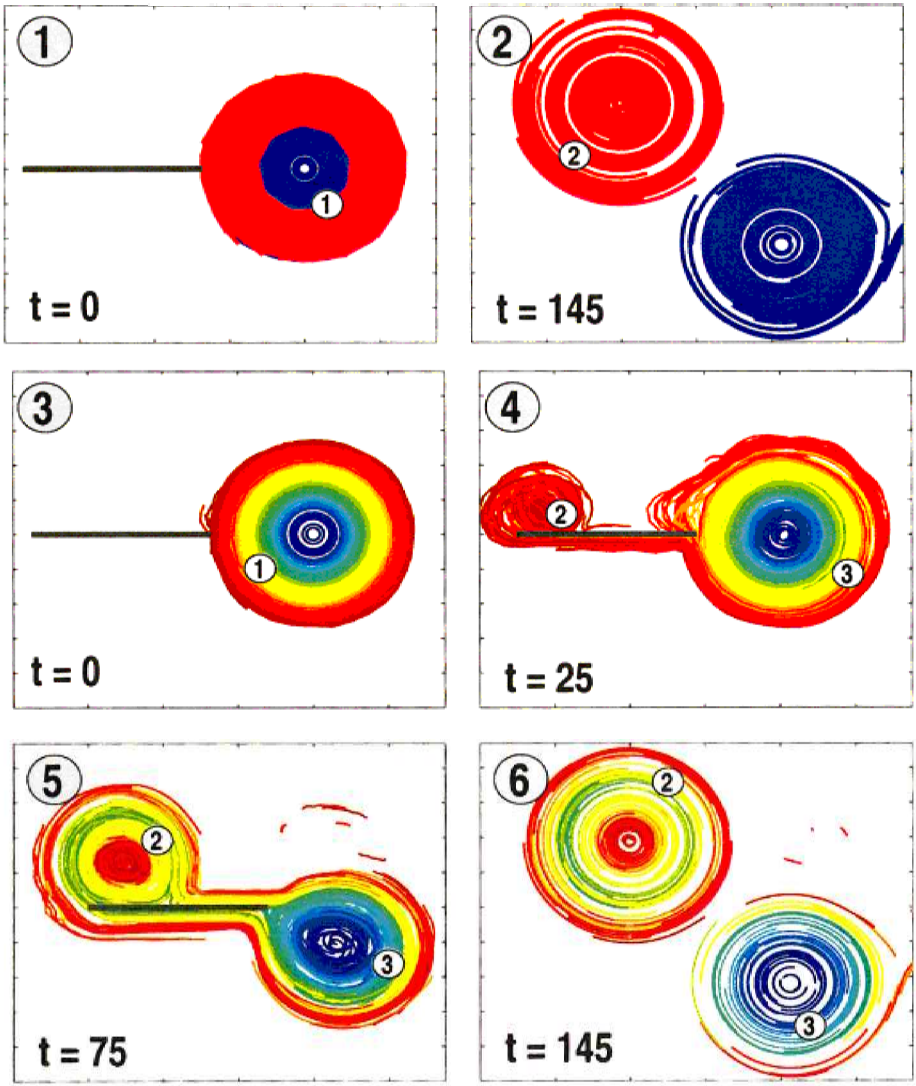

Figure 12. "Dyed" Lagrangian floats "released" in a typical numerical simulation of a lens splitting (experiment 68) reveal how the fluid from the parent lens is distributed in the offspring. In panels 1 and 2, the fluid that ultimately forms lens 2 (3) is dyed blue (red). In panels 3–6, the color pallette has been expanded and is colored according to its initial radius in the parent lens. This reveals that the core fluid of lens 2 is derived from the fluid initially at the very rim of lens 1, whereas the fluid at an intermediate radius in lens 2 is derived from fluid initially at an intermediate radius in lens 1. Additionally, the splitting sequence (panels 3–6) shows that there is some drainage of fluid from lens 2 back to lens 3 during the splitting process so that a "slug" of rim water circulates around both lenses during the encounter with the wall.

of the wall (Fig. 12, panels 4 and 5). This means that the rim fluid of the offspring is derived from a slug of water originating at the very rim of the parent lens. This fluid circulates around both lenses as they are splitting, i.e., there is a continuous circulation around both lenses during the splitting (Fig. 12, panels 5 and 6).

While neither mode was realized precisely as we originally supposed, the numerical experiments confirm that there are clearly two distinct final states (Fig. 11). In the first, the lenses end up on opposite sides of the wall (mode 1), whereas in the second they occupy the same side of the wall (mode 2). For all L, the boundary between the modes occurs at approximately $d/R_1 = -0.45$.

ii. Comparison with the theory (Eqs. 24 and 25). In the top four panels of Figure 10, we compare our numerically determined γ with that obtained from (24). The dashed lines show a multi-valued branch, rejected on the grounds that it cannot be reached because it corresponds to a larger value of γ. We see that indeed, the second value of the analytical solution was never approached by the numerical simulations.

Only experiments which resulted in a splitting outcome are shown. For each value of d, we see that γ was nearly constant (and was above the predicted curve). The agreement improved for d approaching unity. For a given value of d, we found that the agreement in γ also improved as L was progressively reduced. This is because with a reduced L, the final separation between the lenses was also reduced so that the final state was better described by our "kissing" assumption (Fig. 10, panels 5 and 6). The worst agreement between the analytics and the numerics was in the determination of r_2 which, as it turned out, was fairly sensitive to our kissing assumption. This aspect will be demonstrated more clearly in Section 5(b)iv, where we compare the numerics with the general analytical derivation that does not yet contain the kissing assumption. Even at the lowest values of L, our analytical solution remained below the numerically determined value, and thus represents a lower bound on γ.

iii. Evaluation of CIAM (Eq. 4). In order to put our solution in perspective, it is instructive to evaluate the complete, unsimplified CIAM, (Eq. 4) (albeit in a fixed coordinate system so that $C = 0$). For completeness, we choose to show an experiment from set 3 which included β. The results are shown in Figure 13. (Similarly excellent results were obtained in all experiments.) We see that the terms of the CIAM balanced each other almost exactly. After day 50, the two lenses were free of the walls (i.e., τ_h vanishes) and drifted uniformly to the west; the production of CIAM was entirely balanced by the τ_β (as discussed earlier in Section 3). On the other hand, energy is not conserved during the splitting process. While the theoretical energy loss is only 30%, the numerical energy loss was 60%. Since there are no waves capable of radiating the required energy loss in our numerical model the energy loss was accomplished by numerical dissipation. While these frictional effects are greater than expected, they have little effect on the angular momentum budget. Note also that the energy fell off slowly (when compared to the duration of the interaction) indicating that, as

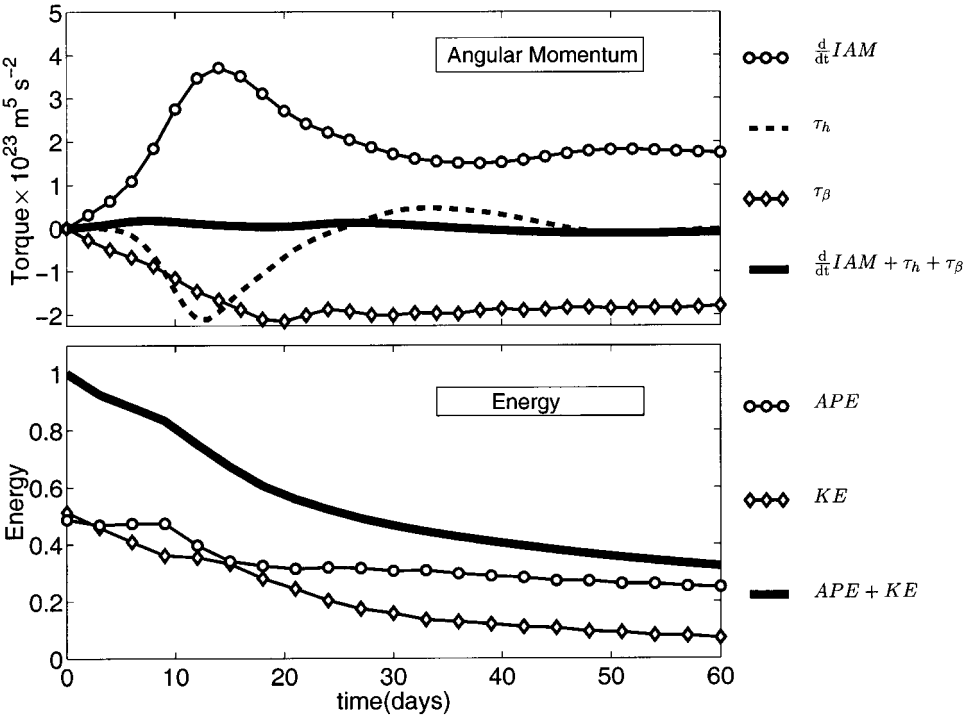

Figure 13. The CIAM budget (4) for a typical lens splitting simulation (set 3, experiment 22). The time rate of change of integrated angular momentum ((*d*/*dt*) IAM), the wall torque (τ_h), and the β-torque (τ_β) very nearly sum up to zero (black line), verifying that CIAM is a reliable constraint. As expected, however, the energy is not conserved. By the time that splitting is completed (day 50 when $\tau_h = 0$), the simulated energy has been reduced (via numerical friction) to 0.4 of the energy at $t = 0$. This 60% frictional loss is somewhat greater than the 30% theoretical energy loss (via radiation).

assumed, the splitting was a slowly varying process rather than a dramatic event. Thus, in contrast to the energy, the full CIAM is an exceedingly strong constraint, even in the dissipative numerical model.

iv. Evaluation of the simplified CIAM (Eq. 18). The first significant stage of simplification to (4) leads us to (18) which relates the final positions of the lenses to the length of the wall. Figure 14 shows an examination of the errors introduced by this first set of simplifications. The main assumption employed up to (18) was that the flow along the wall was geostrophic, and that the migration speed of the wall was much less than the speed of the jet. As mentioned previously, the theoretical value of ε for this slow collision was 0.03. Our scaling for the thickness of the wall jet ($h_w = \varepsilon^{1/2} H_1$) predicted that $h_w \approx 100$ meters; in the numerics, the average thickness of the wall jet during a typical splitting process was 150 meters. Since (18) does an excellent job of relating the final positions of the offspring

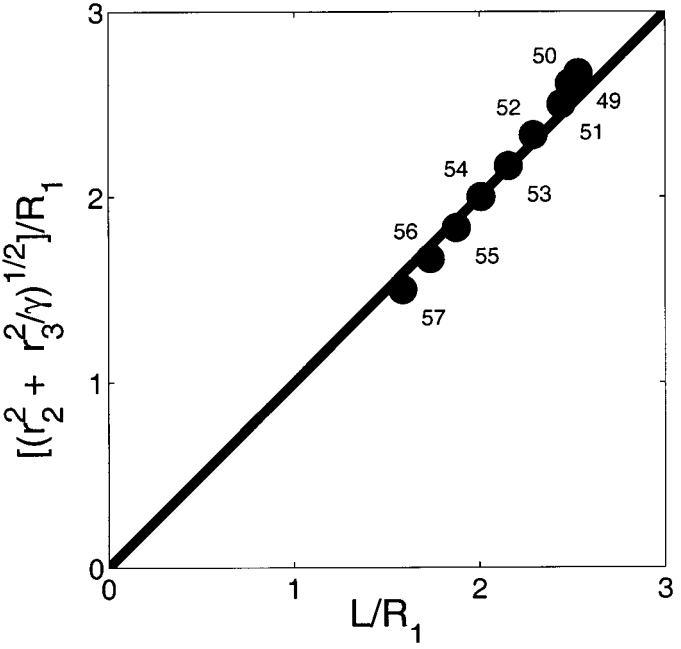

Figure 14. Comparison of the simplified CIAM (solid line, Eq. 18) with several numerical experiments resulting in a split (solid circles). The very close agreement tells us that this extremely simplified form of CIAM is a powerful constraint for the splitting of eddies. For simplicity, we present here experiments 49–57 (from set 1) that correspond to $d/R_1 = -0.2$. (Results for other values of d are very similar.)

to the wall length (and yet does not involve any assumption about the final locations of the lenses), the explanation for the discrepancy seen in (Fig. 10) must lie almost exclusively in our chosen geometric configuration, and not in our integration of (4).

v. A lower bound on wall length capable of splitting a lens. It is worthwhile to determine the lower bound on the wall length capable of splitting a lens. (We shall denote this wall length L_{crit}.) To do so, we recast our analytical solution so as to consider γ as known (Fig. 7 and 8, panel 6). For each value of γ, this defines a curve L vs d (with a definite minima, $L = L_{crit}$, and associated value of d). By stepping through a range of γ, we can then define L_{crit} on the interval $-1 < d/R_1 < 1$ (Fig. 15). When we compare the analytical and numerical value of L_{crit}, we find that the numerical experiments were consistently close to (but above) the analytically determined lower bound (Fig. 16).

The $\gamma = 1$ case deserves special attention because it represents the most dramatic splitting outcome. From the analytical solution, we determine that (for $\gamma = 1$) $L_{crit} = 2^{1/4} \approx 1.19$ occurs at $d = 0$. The outcome from the experiment in set 1 which is closest to this simple solution (experiment 68) is $L_{crit}(d = 0,\ \gamma = 1.1) = 1.7R_1$. Three resolution-

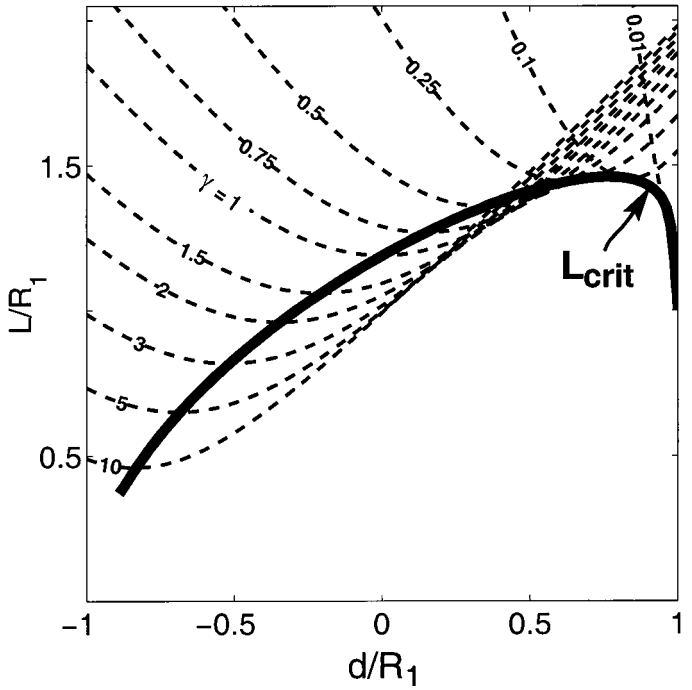

Figure 15. A plot of the critical value of L from our analytical solution (thick black line). The dashed lines are L as a function of d for various values of γ. The curve for L_{crit} was obtained by connecting the smallest possible values that L can take for a given value of γ. Only mode 1 is shown here (L_{crit} for both modes are shown in Section 5).

doubling experiments were also conducted. By iteratively reducing the wall length, we were able reduce the numerically determined lower bound to $L_{crit}(d = 0, \gamma = 1.3) = 1.4R_1$. Thus, at higher resolution, the numerical value of L_{crit} is closer to the analytical lower bound than the corresponding lower resolution value. As expected, it remains above the analytically determined value.

Another significant aspect of our analytical solution was that $\gamma \to 0$ as $d \to \pm 1$ so that, even for the weakest splitting to occur, L must be $O(R_1)$. The most relevant outcomes from the numerical experiments were $L_{crit}(d = 0.89R_1, \gamma = 0.09) = 1.7R_1$ for mode 1, and $L_{crit}(d = -0.89R_1, \gamma = 0.07) = 2.0R_1$ for mode 2 (experiments 6 and 128, respectively). As expected, L_{crit} remained $O(R_1)$ even in the limit of weak collisions.

6. Numerical extensions

Here we present our investigations of lens intensity and β (sets 2 and 3, Table 1). Set 2 was exactly like set 1, except that the lens Rossby number was ¼ (instead of 1), and H_1 was 150 meters (instead of 600 meters). In the experiments of set 3, we examined the effect of β in isolation, i.e., we kept the wall stationary while the lens drifted westward due to β. As in

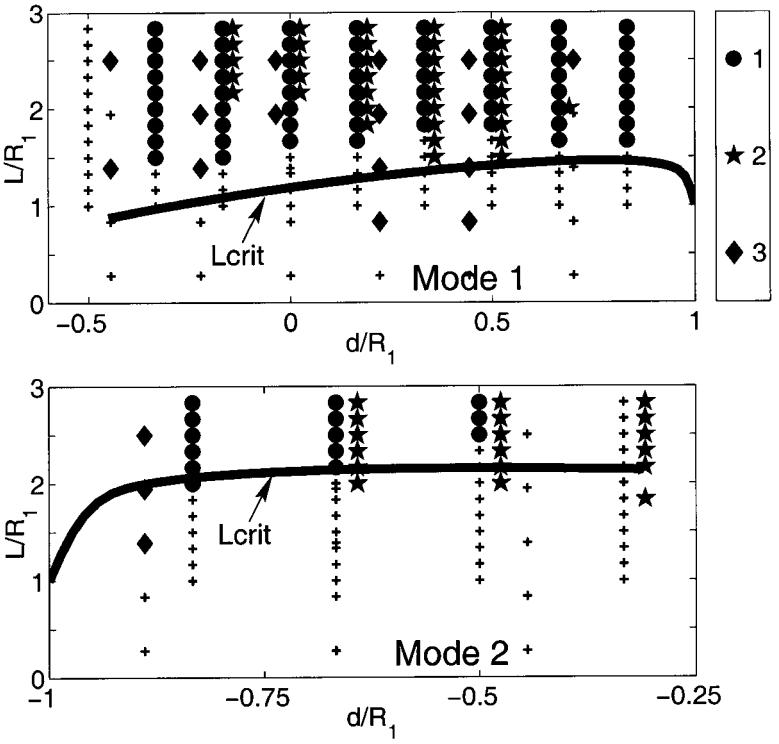

Figure 16. Comparison between the numerical experiments (circle, star, and diamond symbols) and the analytically determined L_{crit} (solid line). The top panel shows numerical experiments which resulted in a "mode 1" type outcome, whereas the bottom panel shows numerical experiments which result in a "mode 2" outcome. The symbol labels refer to the three sets of experiments described in Table 1. Crosses (+) indicate an experiment without splitting, whereas solid circles (set 1), stars (set 2) and diamonds (set 3) indicate experiments where splitting actually occurred. For clarity, stars are slightly shifted by $+0.025R_1$, and diamonds by $-0.025R_1$. For set 1, it is clear that the numerical value of L_{crit} is very close to (but larger than) the analytically determined lower bound. Sets 2 and 3, which focused on a slightly different physical system, generally agree but do show a few small exceptions. Note that as $d/R_1 \rightarrow \pm 1$, L/R_1 remains $O(1)$ for all of the experiments.

set 1, the basic strategy for the execution of sets 2 and 3 was to systematically vary the wall length (L) and the initial contact point between the wall and the lens (d). Since our analytical solution did not include arbitrary Rossby number lenses or β, we limit our discussion to comparisons between L_{crit} derived from our analytical solution and the corresponding value found in set 1.

a. Set 2 (lens intensity)

To examine the role of lens intensity, numerical experiments for $R_o = \frac{1}{4}$ were performed with wall geometries identical to that of set 1 (Table 1). As in set 1, the lens was fixed and

the wall was translating toward it. We found that the basic splitting phenomenon was the same as before but there were systematic differences in the outcome. In particular, the collisions tended to be messier, the final lenses tended to be less axisymmetric, and there was a great deal of "smearing." This may be attributable to differences in the dynamics but may also be due to the fact that the $R_o = 1/4$ lenses experienced more dissipation due to their smaller layer thicknesses.

The "smearing" meant that to "cleanly" split a lens, L_{crit} needed to be somewhat longer than that of comparable experiments in set 1 (Fig. 16). Significant splitting did not occur below $d = -0.67R_1$ or above $d = 0.67R_1$ for any chosen value of L (Fig. 16). Another interesting aspect of the lower amplitude lenses was that the value of d associated with the boundary between mode 1 to mode 2 occurred at $d = -0.33R_1$ (as opposed to $d = -0.45R_1$ found in set 1). All the experiments in set 2 had outcomes with $\gamma < 1$ meaning that less mass was transferred via the wall-jet. Since the total momentum flux to lens 2 (in the negative x-direction) was smaller, lens 3 shifted in the negative y-direction less than in set 1 and could remain in mode 1 (i.e., "above" the wall) for larger values of d.

As in set 1, we looked carefully for outcomes with two (nearly) equal offspring. We found $L_{crit}(d = 0, \gamma = 0.8) = 2.2R_1$ which is somewhat greater than the corresponding set 1 case. When we doubled the resolution we were able to find $L_{crit}(d = 0, \gamma = .9) = 1.5R_1$, which is slightly lower than the $R_o = 1$ numerical result at the standard resolution, but very similar to the set 1 case at higher resolution. It seems that our computational grid resolution is insufficient for these lower amplitude lenses. Thus our study does not resolve the issue of whether or not weaker lenses are more (or less) prone to wall-induced splitting. It does suggest, however, that low resolution representation of lenses tends to suppress splitting.

b. Set 3 (β)

Set 3 was limited to 48 experiments due to the extremely long integration times associated with using β as the collision mechanism. We used an elevated value of $\beta = 6 \times 10^{-13}$ (cm s)$^{-1}$, which forces the lens to drift to the west more rapidly than the standard β. This had the benefit of reducing the integration times (thereby moderating the effects of numerical dissipation). The parameter d took on eight evenly distributed values from −128 km to 96 km ($-0.9R_1$ to $0.7R_1$) and L took on six evenly distributed values from 40 km to 440 km ($0.3R_1$ to $3.0R_1$). Again, focusing on $\gamma = 1$, we found that β allows smaller wall lengths to produce a split [$L_{crit}(d = 0, \gamma = 1.1) = 0.9R_1$, which is 25% lower than the theory admits]. In some cases, however, splitting did not occur even though L was longer than the critical length determined from both the theory and sets 1 and 2 (Fig. 16).

Because the β-induced westward drift rate of a lens is proportional to its intensity, splitting cannot be permanent when $\gamma < 1$. Under such conditions, a weaker lens 2 would be overtaken and re-absorbed from behind by the stronger lens 3 (unless there is no zonal overlap of the lenses along the y-axis). When lens 2 is more intense than lens 3 (i.e., $\gamma > 1$), β can cause splitting even when the lenses are connected by a modest filament (which would otherwise cause them to re-merge). In this case, β induces a growing separation

Table 2. Observations of Meddy splitting or destruction by collision with seamounts. In the first column we give the name of the Meddy used in the study cited, in the second an estimate for the length scale associated with the seamount, in the third the initial radius of the Meddies, in the fourth the ratio L/R_1, in the fifth the outcome, and in the last column, the literature source.

Name	Seamount	L	R_1	L/R_1	Outcome	Study
Meddy 3	Cruiser	35 km	75 km	0.5	split	Richardson and Tychensky (1998)
Meddy 3	Irving	45 km	75 km	0.6	split	Richardson and Tychensky (1998)
Meddy 3	Cruiser + Irving	80 km	75 km	1.1	split	Richardson and Tychensky (1998)
"Irving"	Irving	45 km	40 km	1.1	split	Shapiro *et al.* (1995)
"Irving"	Hyéres	60 km	40 km	1.5	split	Shapiro *et al.* (1995)
Meddy 2	Hyéres	60 km	50 km	1.2	destroyed?	Richardson *et al.* (1989)
unnamed	Cruiser	60 km	50 km	1.2	weak splitting	Dykhno *et al.* (1991)

between the lenses. This accounts for the three exceptions to the minimum splitting criteria seen in Figure 16, and for the experiments where splitting did not occur when we expected that it would. In support of this argument, γ was less than one for only four out of forty-eight experiments in this set. If integration times were longer, none of these splitting outcomes could have been permanent.

7. Oceanic observations of Meddy/Seamount collisions

Here, we relate the present theory to the few observations of direct eddy collisions with isolated topography (Table 2). We limit our discussion to the collision of Meddies with seamounts for which we have the best data. Because the lateral length scale of the seamounts (L) is small relative to the lateral length scales of the Meddies (R_1), the seamounts are like vertical walls (Fig. 1). We will discuss length scales for splitting requiring $L/R_1 \sim O(1)$ because further precision seems unwarranted. As shown in Figure 1, the seamount scales can be easily estimated from their mean diameter at 1050 meters.

Two RAFOS floats embedded in a Meddy encountered Cruiser and Irving Seamounts (Richardson and Tychensky, 1998). One float initially looped around Cruiser and then around both Cruiser and Irving and then continued looping to the north (Figs. 1 and 17). Upon collision with Cruiser Seamount, a second float in the same Meddy headed to the south, suggesting that the Meddy split into two offspring. Based on a Meddy radius of 75 km (one of the largest and most intense ever observed) and Cruiser's diameter of 35 km, we determine that $L/R_1 = 0.5$ for this collision. Using Irving Seamount (45 km in diameter) for a length scale, we get $L/R_1 = 0.6$. Both estimates are somewhat below our analytical lower bound for splitting. However, Irving and Cruiser Seamounts are separated by only 30 km at 1050 meters; if the Meddy received torque from both Cruiser and Irving so that they acted dynamically as a single seamount (with a combined length scale of 80 km), then

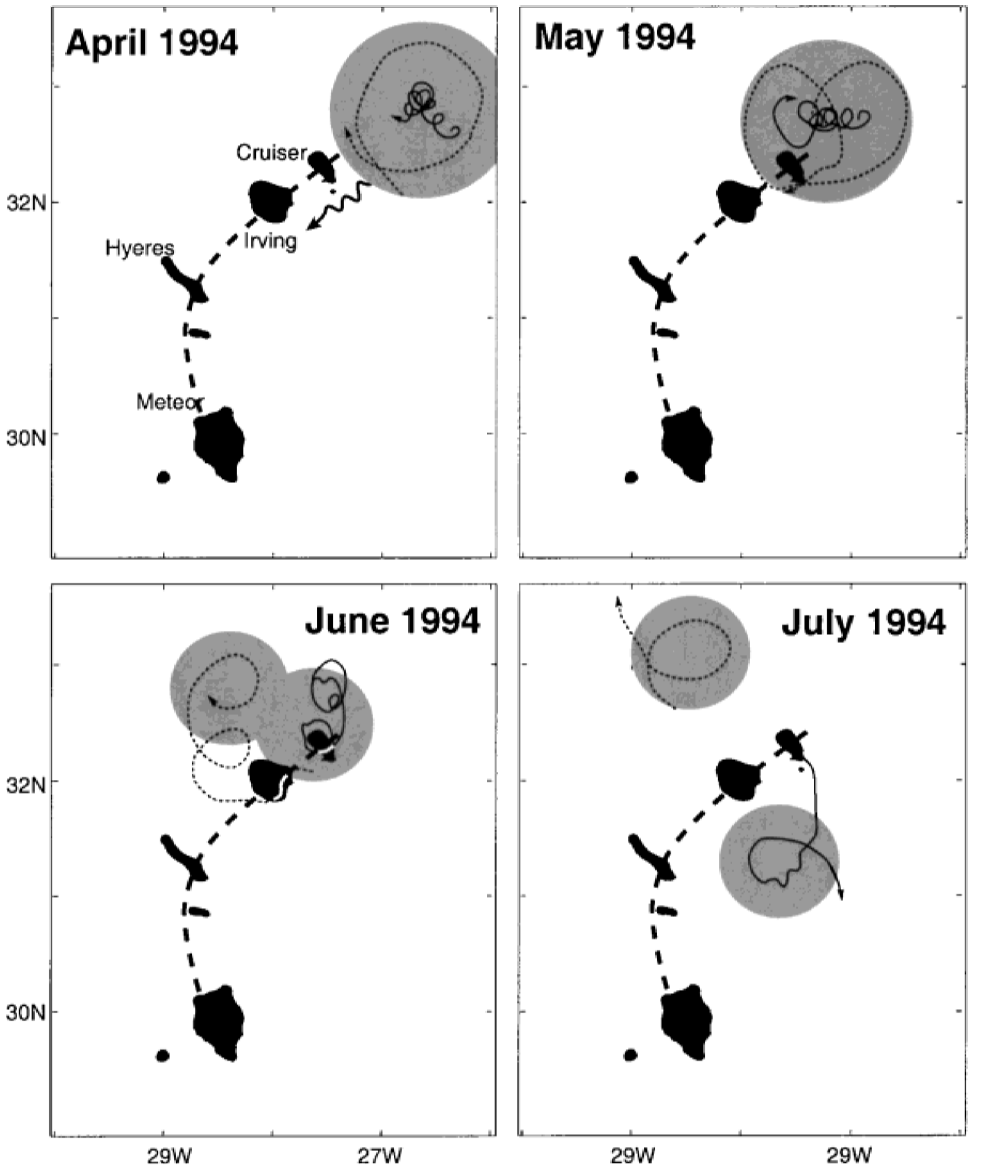

Figure 17. RAFOS float observation of a Meddy collision with the Great Meteor Seamounts (Meddy 3, Table 2). The "wiggly" arrow in the upper left hand panel indicates the initial migration direction of the Meddy. The float trajectories are shown in plan view, with depth above 1050 meters are shown in black. (An alternate view of this collision was shown in Fig. 1.) The thick dashed line represents our conceptual "wall." In the top panels, two floats are trapped in a Meddy (indicated schematically by the grey region). One float is shown as a dotted line, the other as a solid line. By June 1994 (lower left panel), the floats are looping in two separate lenses, and by July, 1994 (lower right panel), the floats have gone in different directions. Richardson and Tychensky (1998) attribute the separation of the two floats to the splitting of the Meddy into two separate offspring upon collision with the seamounts (adapted from Richardson and Tychensky, 1998).

our L/R_1 is 1.1. The fact that the floats circled both Cruiser and Irving (Fig. 17) suggests that it may be reasonable to consider the ensemble of the Great Meteor Seamounts as if it behaves as a single wall (Fig. 1).

Shapiro *et al.* (1995) reported that, upon passing between Hyéres and Irving Seamounts, a Meddy lost 20% of its salt and 27% of its heat excess to a smaller offspring Meddy. As mentioned, at a depth of 1050 meters, Irving Seamount is approximately circular with a diameter of 45 km; Hyéres is long and narrow with a length of 60 km. We find that, for Hyéres Seamount, $L/R_1 = 1.6$, and for Irving, $L/R_1 = 1.1$, so that each individual seamount is potentially large enough to have split the lens by our criteria.

On the basis of two floats (previously embedded in the Meddy) which ceased looping, Richardson *et al.* (1989) concluded that a 50 km radius Meddy was destroyed upon collision with Hyéres Seamount ($L/R = 1.2$). (Note that Hyéres is actually rather long and skinny with an aspect ratio 0.2, so that it is actually very much like the walls analyzed here.) For completeness, the reader is also referred to Dykhno *et al.* (1991), who reported on weak splitting associated with the collision of a 50 km radius Meddy with Cruiser seamount ($L/R_1 = 1.2$), and also to the review article of Richardson *et al.* (2000).

8. Limitations of the analysis

As is the case with any new problem, a number of necessary simplifications have to be made. Specific deficiencies in our study are:

1. *Islands modeled as finite length vertical walls.* Comparison of relative scales suggests that the vertical wall idealization is applicable for many cases (Fig. 1). Nevertheless, topographic effects are certainly central to the dynamics and should be considered as a secondary effect. Analysis of a sloping boundary is beyond the scope of this work.

2. *Neglect of baroclinicity.* The lens model employed here is stable (see, e.g., Killworth, 1983; Flierl, 1984; Hopfinger and van Heijst, 1993). However, Paldor and Nof (1990) showed that a zero PV lens in a finite depth ocean can be unstable when the ocean-lens depth ratio is less than 3 or 4. Note that even with an active lower layer, no torque can be imposed on a feature whose peripheral layer thickness vanishes. Additionally, Nof (1991) showed that for a slow splitting process (i.e., $T_{\text{enc}} \gg f^{-1}$), even a baroclinic anticyclone with non-vanishing peripheral layer thickness cannot split spontaneously because the line integral in (4) remains small. Therefore, slow splitting requires input of torque from a boundary.

3. *Lens model.* We concentrated on a special type of a lens with a velocity profile of the type $v_\theta = -(\frac{1}{2})Rofr$, where $Ro = 1$ corresponds to a zero potential vorticity lens. Although many ocean eddies have been observed to have cores of this type, real ocean eddies are not inviscid lenses. They are embedded in a viscous medium with continuously varying temperature and salinity, so that even when eddies are observed

to have a core in solid body rotation, the velocity decays gradually beyond this inner core. Thus real eddies have far field expression, with associated image effects.

9. Summary

Our aim in this work has been to determine when an island can provide enough torque to break an anticyclonic eddy into at least two parts. [Recall that Nof (1990) demonstrated that anticyclones are prohibited from breaking without a source of external torque.] To do so, we introduced the equivalence between a stationary lens sliced by a slowly moving wall and a lens gradually advected into a stationary wall aligned with the direction of the advecting flow. For this special geometry, it was possible to explicitly solve for the input of torque leading to a split. This enabled us to connect the beginning and end states using conservation of integrated momentum, and thereby determine the final (split) state arising from such a collision.

For the case of the moving (thin) wall on an *f*-plane, the conservation of integrated angular momentum was simplified using the so-called "slowly varying" approach. Specifically, consideration of collisions where $C_{wall}/C_{jet} = \varepsilon \ll 1$ allowed us to reduce the CIAM to a simple relationship between the initial and final locations of the lenses, the volumes, and the length of the wall *L*. Since we do not know *a priori* either the final location of the lenses or the partitioning of mass between the offspring, we introduced a closure condition demanding that the final lenses would be minimally separated (i.e., they would be "kissing") as shown in Figure 6. This allowed us to close the problem and reach our final solution. Numerical experiments revealed that the CIAM is a very strong constraint (Figs. 13 and 14). Since very long walls result in offspring that are widely separated in the final state (i.e., not kissing), our solution provided a lower bound on the mass redistribution resulting from the collision (Fig. 10). Shorter walls (which result in offspring which are closer together) produced better agreement with the numerics than longer walls did.

By recasting our solution in terms of γ, the ratio of the offspring volumes, we obtained the minimum wall length capable of splitting a lens (Fig. 15). This length is referred to as L_{crit}. We found in both the analytical solution and numerical experiments that L_{crit} was $O(R_1)$ for all *d* (Fig. 16), and that the analytically determined value was close to (but above) the numerical outcome (Fig. 16). For splitting into two equal offspring, the analytical solution required a wall length of at least $1.19R_1$; the numerically obtained value was $1.5R_1$. We found that both in the presence of β and for weaker lenses, L_{crit} was above the lower bound as should be the case. On rare occasions it was (moderately) below the theoretical lower bound but, even for these cases, it was always very close to $O(R_1)$ (Fig. 16).

The final detailed structure of the offspring was revealed with the use of Lagrangian floats (Fig. 12). Our analysis shows that the radial position of the fluid in the second lens is inverted relative to its initial radial positioning in the parent lens (Fig. 12, panel 6). (A "slug" of fluid at the very perimeter of the offspring which is derived from the fluid

initially at the rim of the parent lens is an exception.) This is conceptually analogous to winding a thread from a full to an empty spool. The fluid (thread) which is initially at the perimeter of the first lens (spool of thread) makes up the core of the second lens (spool of thread).

Cyclones (which were not considered here) rotate in the same sense as f, and hence their angular momentum exceeds that of anticyclones. Therefore, an external source of torque is not required for breakage to occur. For this reason it is expected that even short walls (small inputs of torque) can instigate the splitting of cyclones. This is supported by the evidence for the preference for cyclone splitting (McWilliams, 1984; Cushman-Roisin and Tang, 1990).

It should be noted that our theory used the analytically tractable simplification that the islands are thin in the dimension orthogonal to the axis defined by the direction of eddy propagation. The radii of the individual seamounts (considered in our comparisons with observations) are comparable to the Meddy's diameter. Additional numerical experiments (not shown) with islands rotated by ninety degrees (i.e., thin walls oriented perpendicular to the axis of eddy propagation) produced very similar results. Thus, the minimum island scale, L/R_1, must always be $O(1)$, regardless of the orientation of the wall.

This is substantiated by the application of our theory to observations of collisions between Meddies and seamounts, where we showed that breakup can result from collisions between Meddies and nearly vertical seamounts with lateral length scales which are $O(R_1)$. This work may have relevance to many other collisions, such as may occur between North Brazil current rings and the Lesser Antilles.

Acknowledgments. This study was supported by the National Aeronatics and Space Administration Earth System Science Fellowship NGT5-30164; the National Science Foundation under contracts OCE 9503816 and 9633655; National Aeronatics and Space Administration grants NAGW-4883 and NAG5-7630; and Office of Naval Research grant N00014-89-J-1606. Discussions with P. Richardson were very helpful.

APPENDIX

List of symbols and terms

List of symbols and terms

PV	Potential vorticity.
β	Linear variation of Coriolis parameter with latitude.
C	Speed of coordinate system in negative x-direction.
g'	Reduced gravity $(\Delta\rho/\rho)g$.
parent	Initial lens.
offspring	Lens(es) derived from a parent lens as a result of a split.
γ	Ratio of offspring lens volumes. By definition, the core of the parent is the denominator, so that γ ranges from 0 to infinity.
r_0	Distance from origin of coordinate system to lens center.
L	Wall length.

L_{crit}	Critical wall length, below which splitting cannot occur.
d	Distance in the y direction from parent lens center to the point where wall first makes contact with the parent lens.
τ_h	Torque due to a wall.
τ_β	Torque supplied by β.
R_1	Initial lens radius.
H_1	Thickness at the center of the parent lens.
f	Coriolis parameter ($f_0 + \beta y$).
h	Upper layer thickness.
h_w	Thickness along the wall.
Δh_w	Thickness difference on opposite sides of the wall.
u, v	Velocities in Cartesian coordinates.
S	Integration area.
IAM	Integrated angular momentum.
CIAM	Conservation of integrated angular momentum.
(d/dt) IAM	Production of integrated angular momentum.
R_o	Lens Rossby number.
v_θ	Azimuthal component of velocity.
V	Lens volume.
Q	Transport by wall jets.
Ro	Rossby number.
A_h	Laplacian friction coefficient in numerical model.
Set	A group of numerical experiments which share some unifying physics.
U_{jet}	Speed at which jet propagates along a wall during a collision between a lens and a wall ($U_{jet} \sim O(\sqrt{g'H_1})$)
T	Total length of time lens(es) and wall are in contact.
T_{enc}	Time scale for encounter between the lens and a wall.
T_{jet}	Time scale for the setup of geostrophic jet along wall.
ε	Ratio of wall speed to orbital speed.

REFERENCES

Armi, L. D., D. Hebert, N. Oakley, J. F. Price, H. T. Rossby and B. Ruddick. 1989. Two years in the life of a Mediterranean salt lens. J. Phys. Oceanogr., *19,* 354–370.

Ball, F. K. 1963. Some general theorems concerning the finite motion of a shallow rotating fluid lying on a paraboloid. J. Fluid Mech., *17,* 240–256.

Bleck, R. and D. Boudra. 1986. Wind-driven spinup in eddy resolving models formulated in isopycnic and isobaric coordinates. J. Geophys. Res., *91,* 7611–7621.

Carnevale, G., R. Kloosterziel and G. van Heijst. 1991. Propagation of barotropic vortices over topography in a rotating tank. J. Fluid Mech., *233,* 119–139.

Cushman-Roisin, B. 1989. On the role of filamentation in the merging of anticyclonic lenses. J. Phys. Oceanogr., *19,* 253–258.

Cushman-Roisin, B. and B. Tang. 1990. Emergence of eddies beyond the radius of deformation. J. Phys. Oceanogr., *20,* 97–113.

Dykhno, L. A., Y. G. Morosov, S. V. Nikitin, B. N. Filyushkin and I. A. Shilov. 1991. Breakup of lenses of Mediterranean water on interaction with bottom relief. Oceanology, *31,* 38–41.

Flierl, G. R. 1984. Rossby wave radiation from a strongly non-linear warm eddy. J. Phys. Oceanogr., *14,* 47–58.

Hopfinger, E. J. and G. J. F. van Heijst. 1993. Vortices in rotating fluids. Ann. Rev. Fluid Mech., *25,* 241–289.

Kamenkovich, V. M., Y. P. Leonov, D. A. Nechaev, D. A. Byrne and A. L. Gordon. 1996. On the influence of bottom topography on the Agulhas eddy. J. Phys. Oceanogr., *26,* 892–912.

Killworth, P. 1983. On the motion of isolated lenses on a beta-plane. J. Phys. Oceanogr., *13,* 368–376.

LaCasce, J. H. 1998. A geostrophic vortex over a slope. J. Phys. Oceanogr., *28,* 2362–2381.

Louis, J., B. Petrie and P. Smith. 1982. Observations of topographic Rossby waves on the continental margin off Nova Scotia. J. Phys. Oceanogr., *12,* 47–55.

Masuda, A. 1986. A skewed eddy of batchelor-modon type. J. Oceanogr. Soc. Japan, *44,* 189–199.

Masuda, A., K. Maribayashi and M. Ishibashi. 1987. Bachelor-modon type eddies and isolated eddies near the coast on an *f*-plane. J. Oceanogr. Soc. Japan, *43,* 383–394.

McWilliams, J. C. 1984. The emergence of isolated coherent vortices in turbulent flow. J. Fluid Mech., *198,* 21–43.

Minato, S. 1982. Geostrophic adjustment near the coast. J. Oceanogr. Soc. Japan, *38,* 225–235.

—— 1983. Geostrophic response near the coast. J. Oceanogr. Soc. Japan, *39,* 141–149.

Mory, M., M. E. Stern and R. W. Griffiths. 1987. Coherent baroclinic eddies on a sloping bottom. J. Fluid Mech., *183,* 45–62.

Nof, D. 1981. On the beta-induced movement of isolated baroclinic eddies. J. Phys. Oceanogr., *11,* 1662–1672.

—— 1988a. Draining vortices. J. Geophys. Astrophys. Fluid Dyn., *42,* 187–208.

—— 1988b. Eddy wall interactions. J. Mar. Res., *46,* 527–555.

—— 1990. The role of angular momentum in the splitting of isolated eddies. Tellus, *42A,* 469–481.

—— 1991. Fission of single and multiple eddies. J. Phys. Oceanogr., *21,* 40–52.

—— 1999. Strange encounters of eddies with walls. J. Mar. Res., *57,* 739–761.

Nof, D. and T. Pichevin. 1996. The retroflection paradox. J. Phys. Oceanogr., *26,* 2344–2385.

Paldor, N. and D. Nof. 1990. Linear instability of an anticyclonic vortex in a two layer ocean. J. Geophys. Res., *95,* 18075, 18075.

Pichevin, T. and D. Nof. 1996. The eddy cannon. Deep-Sea Res., *43,* 1475–1507.

Richardson, P., A. Bower and W. Zenk. 2000. A census of meddies tracked by floats. Progr. Oceanogr., *45,* 209–250.

Richardson, P. L. and A. Tychensky. 1998. Meddy trajectories in the Canary Basin measured during the semaphore experiment, 1993–1995. J. Geophys. Res., *103,* 25029–25045.

Richardson, P. L., D. Walsh, L. Armi, M. Schröeder and J. F. Price. 1989. Tracking three meddies with sofar floats. J. Phys. Oceanogr., *19,* 371–383.

Sanson, L. Z., F. Graef and E. G. Pavia. 1998. Collision of anticyclonic, lens-like eddies with a meridional western boundary. J. Geophys. Res., *103,* 24881–24890.

Shapiro, G. I., S. L. Meschanov and M. V. Emelianov. 1995. Mediterranean lense "Irving" after its collision with seamounts. Oceanology Acta, *18,* 309–318.

Shi, C. and D. Nof. 1993. The splitting of eddies along boundaries. J. Mar. Res., *51,* 771–795.

Simmons, H. and D. Nof. 2001. The squeezing of eddies. J. Phys. Oceanogr. (submitted).

Smith, D. C. and J. J. O'Brien. 1983. The interaction of a two layer isolated mesoscale eddy with topography. J. Phys. Oceanogr., *12,* 1681–1697.

Smith, W. H. F. and D. T. Sandwell. 1997. Global seafloor topography from satellite altimetry and ship depth soundings. Science, *277*(5334), 1956–1962.

Stern, M. 2000. Scattering of an eddy advected by a current towards a topographic obstacle. J. Fluid Mech., *402,* 211–223.

Swaters, G. E. and G. Flierl. 1991. Dynamics of ventilated coherent cold eddies on a sloping bottom. J. Fluid Mech., *223,* 565–587.

Umatani, S. and S. M. T. Yamagata. 1982. Geostrophic adjustment near the coast. J. Oceanogr. Soc. Japan, *43,* 197–203.

Velasco Fuentes, O. U. and G. F. van Heijst. 1994. Experimental study of dipolar vortices on a topographic β-plane. J. Fluid Mech., *259,* 76–106.

Yasuda, I., K. Okuda, and K. Mizuno. 1986. Numerical study on the vortices near boundaries: Considerations on warm core rings in the vicinity of east coast of Japan. Bull. Tohuku Reg. Fish. Res. Lab., *48,* 67–86.

Zalesak, S. T. 1979. Fully multidimensional flux-corrected transport algorithms for fluids. J. Comp. Physics, *31,* 335–362.

Received: *23 May, 2000;* revised*: 14 September, 2000.*